TECHNICAL MEMORANDUM

274

The numerical coupling of the physical parametrizations to the "dynamical" equations in a forecast model

N.P. Wedi

Research Department

March 1999

European Centre for Medium-Range Weather Forecasts
Europäisches Zentrum für mittelfristige Wettervorhersage
Centre européen pour les prévisions météorologiques à moyen

The Numerical Coupling of the Physical Parameterizations to the "Dynamical" Equations in a Forecast Model

by **Nils Peter Wedi**

Abstract

A revised coupling of the physical parameterizations to the "dynamical" model equations in the Integrated Forecasting System (IFS) at ECMWF is described and compared with the current operational configuration. The revision called SLAVEPP (Semi-Lagrangian Averaging of Physical Parameterizations) consists of two parts. The tendencies of the parameterizations are averaged within the semi-Lagrangian framework by evaluating part of the "physics" at the arrival point and the remainder at the departure point of the trajectory. Furthermore, the coupling of the different parameterization schemes to each other is changed using a preliminary predicted value of the model's dynamic variables as input to the parameterizations. This predictor is derived from the contributions of radiation, convection and cloud parameterization of the previous time-step and vertical diffusion and gravity wave drag parameterization at the current time-step.

The new method SLAVEPP

- *is second order accurate with regard to the "averaged" parts of the parameterizations. The current operational configuration is only first order accurate.*
- *is stable. A potential instability remains due to the current handling of the gravity wave drag parameterization. Further experimentation has been done indicating that this could be removed by adding it to the "averaged" part of the parameterizations. A simplified stability analysis also indicates that the current operational configuration is potentially unstable.*
- *reduces the dependence on the time-step and the dependence on the calling sequence of the physical parameterizations with respect to the "dynamical" part. It may allow an increase of the used time-step.*
- *reduces numerical noise caused by the parameterizations or the coupling of the parameterizations to the "dynamics".*
- *improves the mass conservation in two case studies (NH winter and summer) of seasonal forecasts over a period of 3 month.*
- *produces more accurate forecasts with respect to the analysis measured in root mean square error and anomaly correlation in various resolutions.*
- *resulted in a more accurate tracking of a tropical cyclone using a T_L639 forecast model with an increased time step.*
- *reduced the large bias in the rainfall prediction compared to observations in two case studies.*
- *improves the coupling to the wave model.*
- *increases the memory requirements by approximately 12 percent with almost no additional computational cost.*

1.0 Introduction

Increased resolution in current NWP models and the use of large time-steps using at least second-order accurate advection schemes stresses the need for an equally accurate computation in time and space of the corresponding physical parameterizations. Semi-Lagrangian advection of the "dynamical" fields (Staniforth and Côté, 1991) is widely used in operational global NWP models. Various first-order accurate methods of coupling these "dynamic" equations with the physical parameterizations are described in the literature (Beljaars, 1991, McDonald, 1992, Moorthi, Higgins and Bates, 1995). Ideally, one would like to evaluate the "physics" terms in the same semi-Lagrangian way, thus resolving the implicit physics' contributions in the solution of the Helmholtz equation of the model variables. McDonald refers to this form of solution as the "holy grail" (McDonald, 1998). However, due to the diffusive nature of the mostly parabolic equations in the physics (Beljaars,1991) this is difficult to achieve. Even without the requirement to use large time steps in order to save CPU time it is rather difficult to find a solver for the equation that includes all the terms of the "physics" directly and such an approach may be too expensive for a spectral model. In most applications two approaches are used to ensure stability for large time-steps. The "dynamics" part of the equations is computed separately from the "physics" and part of the parameterized equations are solved implicitly (McDonald, 1998). Semi-Lagrangian models using a formally second-order accurate treatment of the parameterizations are presented by Williamson and Olsen (1994) for a three-time-level and by Grabowski and Smolarkiewicz (1996) for a two-time-level version. Evaluating the forcing terms resulting from the parameterizations at the departure point and at the arrival point of the semi-Lagrangian trajectory ensures the second-order accuracy of the method (Grabowski and Smolarkiewicz, 1996). In the present study a partially second-order accurate approximation of the physical parameterizations in the two-time-level-version of the IFS model at ECMWF is also achieved by averaging part of the parameterizations tendencies "along" the semi-Lagrangian trajectory. The vertical diffusion part of the parameterizations is only computed at the arrival point (therefore only first order accurate in time and space) because large errors have been found in the vicinity of orography in the lowest model level.

NWP models commonly include physical parameterizations of radiation, turbulent vertical diffusion of heat, moisture and momentum, gravity waves, convection and clouds. Different approaches are used (McDonald,1998, Beljaars, 1991) to couple these various parameterization schemes together. The IFS model at ECMWF computes the parameterizations in the order given above starting with radiation. The vertical diffusion and the gravity wave parameterization use the information that the radiation has changed the temperature field. In the same way Convection and cloud parameterizations use the model variables updated by the previous processes. This is called the fractional stepping method (Beljaars, 1991). However, this method introduces a time-step dependency as "intermediate" model variables are used to compute the successive part of the parameterizations. SLAVEPP uses a "first-guess" predictor value based on the contributions of the parameterizations of the previous time-step and of the current time-step. This ensures the evaluation of each individual parameterization at a full time-level and thus makes the result less time-step dependent. This is highly desirable in an operational environment like ECMWF, where the same model is run with different resolutions and different time-steps for different applications.

The paper is organized as follows. Section 2.1 explains the general framework of the two time-level semi-Lagrangian scheme and describes the revised scheme of coupling the dynamics to the physical parameterizations. Section 2.2 discusses the problem of coupling the various parameterizations to each other. Section 2.3 performs a simplified stability analysis on an advection-diffusion equation as used in the IFS. Section 3.0 discusses the results achieved with the revised scheme compared to observational data and compared to the operational configuration. Section 4.0 summarizes the results and presents some concluding remarks.

2.0 Description of revised numerical scheme

2.1 Coupling of parameterizations with the "dynamics"

Following *Staniforth and Coté* (1991) the forced advection problem of a scalar field F is given by

$$\frac{d}{dt}F(\vec{x},t)+G(\vec{x},t) = R(\vec{x},t) \quad , \tag{2.1.1}$$

where

$$\begin{aligned}\frac{dF}{dt} &= \frac{\partial}{\partial t}F+\vec{V}(\vec{x},t)\cdot\nabla F \\ \frac{d}{dt}\vec{x} &= \vec{V}(\vec{x},t)\end{aligned} \tag{2.1.2}$$

The corresponding semi-Lagrangian two-time-level approximation in discretized form gives

$$\frac{F^{+}-F^{0}}{\Delta t}+\frac{1}{2}[G^{+}+G^{0}] = R^{1/2}, \tag{2.1.3}$$

where the superscripts ($^{+}$, $^{1/2}$, $^{-}$) denote respectively an evaluation at the arrival point $(\vec{g},t+\Delta t)$, the midpoint $(\vec{g}-\vec{\alpha}/2,\,t+\Delta t/2)$ and the departure point of the trajectory $(\vec{g}-\vec{\alpha},t)$. Here $\vec{g}$ is the position vector at the arrival gridpoint, $\vec{g}-\vec{\alpha}$ is the position vector at the departure point and G(linearized) and R(non-linear) specify forcing terms. This scheme is second-order accurate in time and space if the estimate for the trajectory calculation is second-order accurate. *Staniforth and Coté (1991)* give the following equations for the vector displacements $\vec{\alpha}$:

$$\vec{\alpha} = \Delta t\vec{V}^{*}(\vec{g}-\vec{\alpha}/2,\,t+\Delta t/2) \tag{2.1.4}$$

interpolating to the midpoint of the trajectory using the extrapolation in time

$$\overrightarrow{V}^{*}(\vec{g},t+\Delta t/2) = \left(\frac{3}{2}\right)\vec{V}(\vec{g},t)-\left(\frac{1}{2}\right)\vec{V}(\vec{g},t-\Delta t)+[O((\Delta t)^{2})]. \tag{2.1.5}$$

Hortal (1998) proposed a different approach based on a second order Taylor expansion about the departure point. In his approach the trajectory (in space) of the present time step is used with the values for the wind components of the previous time step to write:

$$\begin{aligned}\overrightarrow{V}^{*}(AV,t+\Delta t/2) &\approx \overrightarrow{V}^{*}(AV,t-\Delta t/2) \\ &= \vec{V}(\vec{g}-\vec{\alpha},t)+\frac{\Delta t}{2}\left(\frac{\vec{V}(\vec{g},t)-\vec{V}(\vec{g}-\vec{\alpha},t-\Delta t)}{\Delta t}\right)+[O((\Delta t)^{2})]\end{aligned} \tag{2.1.6}$$

AV denotes an average along the trajectory rather than an interpolation to the midpoint. If physical parameterizations are included there is an additional forcing term P in equation (2.1.1)

$$\frac{d}{dt}F(\vec{x},t)+G(\vec{x},t) = R(\vec{x},t)+P(\vec{x},t). \tag{2.1.7}$$

Discretization with a second-order approximation of P leads to

$$\frac{F^{+}-F^{0}}{\Delta t}+\frac{1}{2}[G^{+}+G^{0}] = R^{1/2}+P^{1/2}. \tag{2.1.8}$$

Using a Taylor expansion of term P around the midpoint of the trajectory gives an estimate for the value of P:

$$\begin{aligned} P^{+}(t+\Delta t,\vec{g}) &= P^{1/2}\left(t+\frac{\Delta t}{2},\vec{g}-\frac{\vec{\alpha}}{2}\right)+\frac{\Delta t}{2}\left(\frac{dP}{dt}\right)^{1/2}+\left(\frac{\Delta t}{2}\right)^{2}\left(\frac{d^{2}P}{dt^{2}}\right)^{1/2}+[O((\Delta t)^{3})] \\ P^{0}(t,\vec{g}-\vec{\alpha}) &= P^{1/2}\left(t+\frac{\Delta t}{2},\vec{g}-\frac{\vec{\alpha}}{2}\right)-\frac{\Delta t}{2}\left(\frac{dP}{dt}\right)^{1/2}+\left(-\frac{\Delta t}{2}\right)^{2}\left(\frac{d^{2}P}{dt^{2}}\right)^{1/2}+[O((\Delta t)^{3})] \end{aligned} \tag{2.1.9}$$

Adding the equations in (2.1.9) leads to the second-order accurate trapezoidal rule approximation computing half of the tendency at the arrival point and half at the departure point of the trajectory:

$$P^{1/2}\left(t+\frac{\Delta t}{2},\vec{g}-\frac{\vec{\alpha}}{2}\right) = \frac{1}{2}[P^{+}(t+\Delta t,\vec{g})+P^{0}(t,\vec{g}-\vec{\alpha})]+[O((\Delta t)^{2})]. \tag{2.1.10}$$

Some NWP models (including the 1998 operational configuration at ECMWF) use only the first term in the Taylor expansion of equation (2.1.9) and evaluate the tendencies from the parameterizations either at the arrival point or the departure point of the trajectory thus are only first order accurate. If the parameterizations are computed at the arrival gridpoint the dependence of the parameterizations on the model variables can be generally written as

$$\frac{F_{P}^{+}-F(t)}{\Delta t} = P^{+}(F_{P}^{+},\tilde{D},F(t)). \tag{2.1.11}$$

F_{P}^{+} is the updated value of the model variables with respect to the parameterizations (partly implicitly solved). $\tilde{D}$ in the 1998 operational IFS model denotes the "dynamic" tendencies as computed by

$$\frac{\tilde{F}_{D}^{+}-F^{0}}{\Delta t}+\frac{1}{2}[\tilde{G}^{+}+G^{0}] = R^{1/2}, \tag{2.1.12}$$

with

$$\tilde{D} = \frac{\tilde{F}_{D}^{+}-F(t)}{\Delta t}. \tag{2.1.13}$$

The "~" denotes that only provisional values of the dynamic fields are available because semi-implicit correction terms are still to be computed (*Hortal, 1991*). Note, that $\tilde{G}^{+}$ denotes an evaluation of the linearized term G at the arrival point but at the present time step. Equation (2.1.13) describes local tendencies, which are computed subtracting the new provisional explicit values $\tilde{F}_{D}^{+}$ of the dynamic fields (at the arrival point) from their values $F(t)$ at the previous time step. These tendencies are then input to the physical parameterizations *(Hortal, 1991)* together with the values of the dynamic fields at the previous time step.

Adding the contributions gives for the 1998 operational IFS model

$$\tilde{F}^{+} = F^{0} - \frac{\Delta t}{2}[\tilde{G}^{+} + G^{0}] + \Delta t R^{1/2} + \Delta t P^{+} \; . \tag{2.1.14}$$

As can be seen from equation (2.1.8), (2.1.9) and (2.1.14) this method is only first order accurate in time and space. If equation (2.1.10) is applied in equation (2.1.8) a second order accurate treatment of the physical parameterizations can be easily achieved:

$$\frac{\tilde{F}^{+} - F^{0}}{\Delta t} + \frac{1}{2}[\tilde{G}^{+} + G^{0}] = R^{1/2} + \frac{1}{2}P^{0} + \frac{1}{2}P^{+} \tag{2.1.15}$$

Equation (2.1.15) leads to:

$$\tilde{F}^{+} = \left[F - \frac{1}{2}\Delta t G + \frac{1}{2}\Delta t P\right]^{0} + \Delta t R^{1/2} + \frac{1}{2}\Delta t[P - \tilde{G}]^{+} . \tag{2.1.16}$$

This approach is used by Williamson and Olsen in the three-time level version of the NCAR Community Climate Model (Williamson and Olsen, 1994). *Grabowski and Smolarkiewicz (1996)* have presented a two-time level semi-Lagrangian model of precipitating clouds ensuring the second-order accurate treatment of the relevant "physical" processes using the same method.

Difficulties were encountered when applying an averaging on all parameterizations in the same manner. These issues are discussed further in section 3.2. Those considerations suggest the following scheme. Equation (2.1.10) is modified to average only radiation, convection and cloud parameterization in time and space while the contributions of vertical diffusion and parameterized gravity waves are taken at the arrival point only:

$$P^{1/2} = \frac{1}{2}P^{0}_{rad+conv+cloud} + \frac{1}{2}P^{+}_{rad+conv+cloud} + P^{+}_{vdif+gwdrag} \tag{2.1.17}$$

which gives with (2.1.8)

$$\tilde{F}^{+} = \left[F - \frac{1}{2}\Delta t G + \frac{1}{2}\Delta t P_{rad+conv+cloud}\right]^{0} + \Delta t R^{1/2} + \frac{1}{2}\Delta t[P_{rad+conv+cloud} - \tilde{G}]^{+} + \Delta t P^{+}_{vdif+gwdrag} \tag{2.1.18}$$

The equation is formally identical to the "holy grail" proposed by McDonald (McDonald, 1998). The ~ denotes that only provisional values are used for F and G, but the resulting P using those provisional values is taken as the true value at time level $t+\Delta t$ at the arrival point. It is a compromise to avoid the additional complication of having to compute semi-implicit corrections for the physics in the ensuing Helmholtz equation that would be far more complicated than the current one. In order to visualize the proposed changes Fig. 7.1-1 shows a typical time step in the two time-level semi-Lagrangian scheme highlighting the differences to the current operational configuration.

2.2 Coupling of the parameterization schemes

The 1998 operational scheme at ECMWF uses the approach of "fractional stepping" (Beljaars, 1991) which uses the information of every parameterized process as input to the next process. The results therefore depend on the sequence in which the processes are called but it ensures a reasonable balance between the dynamical and the physical terms and the physical terms between each other. Other models such as the ARPEGE/IFS model at Meteo

France compute each parameterization independently from each other at time level t avoiding the complication of coupling. The method of "fractional stepping" has the disadvantage that it introduces a time-step dependency as "intermediate" time levels are used when the fields are updated process by process starting with the input from the "dynamics". Therefore, it is suggested to keep the idea of "fractional stepping" but to use a "first guess" predictor of the model variables at the arrival point evaluated by using the tendency from the "dynamics", the tendency of the parameterizations of radiation, convection and clouds at the previous time-step and the tendency of vertical diffusion and gravity waves at the current time-step:

$$F^{+}_{predict} = \tilde{F}^{+}_{D} + P^{0}_{rad+conv+cloud}\Delta t + P^{+}_{vdif+gwdrag}\Delta t\,. \tag{2.2.1}$$

In the proposed scheme the parameterizations at the current time-step are computed in the following calling sequence:

$$\begin{aligned} P^{+} = {} & P^{+}_{rad}(F(t)) \\ & + P^{+}_{vdif}(F(t), \tilde{D}, P^{+}_{rad}) \\ & + P^{+}_{gwdrag}(F(t), \tilde{D}) \\ & + P^{+}_{conv}(F^{+}_{predict}, (output)X_{conv}) \\ & + P^{+}_{cloud}(F^{+}_{predict}, (input)X_{conv}) \end{aligned} \tag{2.2.2}$$

where X_{conv} denotes some convective parameters *(output)* that are explicitly used as *(input)* in the cloud parameterization scheme and $\tilde{D}$ denotes the update with respect to the "dynamics" (as described in (2.1.13)). The current operational model at ECMWF uses "full fractional stepping" as shown in the following equation:

$$\begin{aligned} P^{+} = {} & P^{+}_{rad}(F(t)) \\ & + P^{+}_{vdif}(F(t), \tilde{D}, P^{+}_{rad}) \\ & + P^{+}_{gwdrag}(F(t), \tilde{D}) \\ & + P^{+}_{conv}(F(t) + \tilde{D}\Delta t + P^{+}_{rad}\Delta t, (output)X_{conv}) \\ & + P^{+}_{cloud}(F(t) + \tilde{D}\Delta t + P^{+}_{rad}\Delta t + P^{+}_{conv}\,\Delta t, (input)X_{conv}) \end{aligned} \tag{2.2.3}$$

Note, that the radiation scheme is left unchanged. This is partly due to technical difficulties to change the radiation scheme consistently. First trials gave worse results when changing the input to use the predictor value of F in the radiation. The vertical velocity is used as input to the convection and could be recomputed solving the continuity equation using the predictor values at the arrival point of the trajectory. This is also not done partly due to technical difficulties in the IFS. The presented results in section 3.0 left the vertical velocity unchanged. Therefore, there is no difference compared to the current operational configuration with respect to the vertical velocity.

The specification of the advection of cloud liquid water and ice is related to the question of how to couple these parameterizations to the dynamics. In the current operational model cloud liquid water and ice are advected separately (basically just interpolated to the departure point) and then added together in the corresponding cloud parameterization routine which acts on the sum. The temperature at the arrival point is then finally used to diagnose the fractions of liquid water and ice which increment the corresponding model variables. With SLAVEPP tendencies for cloud liquid water and ice originate from different time levels and partly from the departure point and partly from the arrival point. If these variables are advected (interpolated) separately they carry information from the temperature of the previous time-step. However, only the temperature at the arrival gridpoint should diagnose the dif-

ferent phases. If half of the tendencies result from the departure point and the previous time-step and half from the arrival point and the current time step an implicit advection of ice and/or liquid water is introduced because one part is evaluated using the wrong temperature. This effect was seen in a three month integration where a significant cooling in the subtropics developed caused by increased amounts of ice and/or liquid water advected from the tropics. Therefore, in the new method SLAVEPP the total amount of liquid water is interpolated to the departure point before any phase changes are diagnosed. In the cloud parameterization the trapezoidal rule (as shown in equation (2.1.10)) is applied to the contribution from the current time-step at the arrival point and the interpolated quantity. The separation into liquid water and ice is done after this averaging based on the predictor value of temperature at the arrival point.

In summary equation (2.2.3) proposes the following changes:

- Use a predictor value for the model variables temperature, humidity, cloud fraction, cloud liquid water and ice and the horizontal wind components.
- Remove the indirect coupling of convection and clouds via the "fractional step"
- Reduce the time-step dependency via introducing a predictor value rather than using "intermediate" time levels thus evaluating convection and clouds at a full time level.
- Advect the sum of cloud liquid water and ice (before phase changes) and use the predictor value of temperature to diagnose the different phases.

2.3 Simplified stability analysis of an one-dimensional advection-diffusion equation

The stability of the revised scheme can be compared to the stability of the current operational configuration in a simple one dimensional advection equation coupled with a term to model the effect of the physical parameterizations. The presented analysis follows closely the ideas of Geleyn (1998). The equation is given by

$$\frac{\partial \psi}{\partial t} + u\frac{\partial \psi}{\partial x} = K\frac{\partial^2 \psi}{\partial x^2}. \tag{2.3.1}$$

If the "physics" part is treated implicitly and a semi-Lagrangian scheme is used for the advection terms the following discretization results:

$$\psi^{t+\Delta t} = \psi^{D} + K\Delta t\frac{\partial^2 \psi^{t+\Delta t}}{\partial x^2}. \tag{2.3.2}$$

ψ^{D} denotes the "dynamical" part. The advection velocity u and the diffusion coefficient K are taken as constant for simplicity. For a monochromatic wave

$$\psi(x,t) = \tilde{\psi}(t)e^{ikx}, \tag{2.3.3}$$

where ~ denotes the complex coefficient of ψ, equation (2.3.2) leads to

$$\tilde{\psi}^{+} = \tilde{\psi}' - k^2K'\Delta t\tilde{\psi}', \tag{2.3.4}$$

where

$$K' = \frac{K}{1 + k^2 K \Delta t}.$$

The following notation is introduced:

$$\begin{aligned} \psi^t &\rightarrow \tilde{\psi}^- \\ \psi^D &\rightarrow \tilde{\psi}' \\ \psi^{t+\Delta t} &\rightarrow \tilde{\psi}^+ \end{aligned} \quad . \tag{2.3.5}$$

The form of equation (2.3.4) is a realistic example of how the "physics" (second part of the r.h.s) is coupled to the "dynamics" (first part of the r.h.s.). If the two parts are treated separately, there are several choices for the variable $\tilde{\psi}'$ in the "physics" part. It should be noted, that up to this point equation (2.3.4) can refer to either scheme, SLAVEPP, evaluating the physics at the arrival point only (as in the current operational scheme) or evaluating the physics at the departure point. Introducing the damping factor D and the Courant number C the current operational scheme - computing the physics at the arrival point only - gives

$$X = \tilde{\psi}^+ / \tilde{\psi}^- = e^{-iC}(1 - De^{iC(1-\delta)}), \tag{2.3.6}$$

with

$$\begin{aligned} D &= k^2 K' \Delta t \leq 1 \\ C &= ku\Delta t \\ \tilde{\psi}' &= \tilde{\psi}^- e^{-i\delta C} \\ 0 &\leq \delta \leq 1 \end{aligned} \quad . \tag{2.3.7}$$

$\delta = 0$ describes the situation where the parameterizations are evaluated at the arrival point but using only values at time level t whereas $\delta = 1$ describes the situation of the physics at the arrival point using the update by the dynamics (in this case a simple advection of a monochromatic wave with constant u). Evaluating the absolute value of the complex expression in (2.3.6) gives

$$\|X\| = \sqrt{1 + D^2 - 2D\cos(C(1-\delta))}. \tag{2.3.8}$$

It follows from the condition for stability $\|X\| \leq 1$ and equation (2.3.8) that the case $\delta = 1$ is stable and the case $\delta = 0$ is unstable if the Courant number becomes large enough that the cosine vanishes. The IFS model at ECMWF uses currently a mixture of the two cases depending on the parameterization type ($\delta = 0$ e.g. gravity wave drag parameterization and $\delta = 1$ e.g. vertical diffusion) and is therefore potentially unstable.

Introducing the parameters α (split the "physics" between departure and arrival point) and β (part of the "physics" that is only computed at the arrival point) the SLAVEPP scheme can be described as

$$X = \tilde{\psi}^+ / \tilde{\psi}^- = e^{-iC}(1 - D[(1-\gamma) + \gamma e^{iC(1-\delta)}]) \tag{2.3.9}$$

with $\gamma = (1-\beta)\alpha$. This assumes that the "physics" that are computed at the arrival point only use the update by the dynamics rather than values at time level t. If $\alpha = 0.5$ the absolute value of X can be derived to

$$\|X\| = \sqrt{(1-D)^2 + D[1-\cos(C(1-\delta))]\left(1-\beta-\frac{D}{2}(1-\beta^2)\right)}. \qquad (2.3.10)$$

For arbitrary parameters β, φ, D with $0<\beta<1$; $0\le\varphi = C(1-\delta)\le\pi$; $0\le D\le 1$ it can be shown numerically that independent of C and δ there is no combination that satisfies the equation $\|X\| > 1$. Therefore, this scheme is absolutely stable, independent of the chosen Courant number (neutral in the case D = 0).

A stability analysis of a scheme that assumes that the part of the "physics" which is computed only at the arrival point using a mixture of values at time level t and an update by the dynamics results in a potential instability. This shows that also with the new scheme SLAVEPP care has to be taken which input values are used in the part that is computed only at the arrival point. It is a requirement for stability that this part has $\delta = 1$ whereas it is shown above that it is irrelevant in the part that is split over two time-steps (e.g. any $0\le\delta\le 1$ is valid). For stability reasons this strongly suggests to either average the tendency of the gravity wave drag parameterization "along" the trajectory or using an update by the dynamics. Further experimentation is therefore needed to investigate both cases.

Note, that using a first guess predictor value for the averaged parameterizations as described in section 2.2 and its impact is not considered here explicitly and as can be seen is not required for stability. Nevertheless, experiments have shown that it is important for the overall performance and accuracy of the scheme to apply those changes, too.

3.0 Results

In the following studies the revised scheme SLAVEPP is compared to control forecasts using the operational configuration as in 1998 (CONTROL). It should be noted that all of the methods using (2.1.10) require an interpolation of the diabatic tendencies P to the departure point of the semi-Lagrangian trajectory. Both linear and cubic interpolation have been tested to assess the impact on forecast skill and the level of computational noise. Only marginal differences have been found on the forecast skill. However, a linear interpolation of the extra term P gives less noise compared to the cubic interpolation method. Hence, (2.1.10) is used in conjunction with a linear interpolation of the term P to the departure point.

In the first model time step are no parameterization tendencies available from the previous time step. Therefore, compared to the CONTROL method, in the first time step the indirect contribution of the radiation to the temperature tendency is missing as input to the cloud and convection parameterization. However, experiments comparing the global mean values of selected convective and cloud parameters at step 0 and step 1 show little or no difference. Therefore, the start-up of the model is assumed to be the same in both methods.

3.1 Comparison of numerical accuracy

"Lax's Equivalence Theorem: Given a properly posed initial value problem and a finite difference approximation to it that satisfies the consistency condition, stability is the necessary and sufficient condition for convergence" (Richtmyer, Morton, 1967). The accurate numerical solution converges in this case to the true solution with infinitely small time-step. Unfortunately, the above theorem cannot be applied to the three dimensional Navier-Stokes equations used in the IFS model. First of all there is no theorem that proofs the existence or the uniqueness of a true solution of these equations. Therefore, it is not a "properly posed initial value problem". As the IFS model uses a series of spherical harmonics to discretize the variables in the Navier-Stokes equations it is possible to proof the consistency condition for the model equations under the assumption that the physical fields do not have any discontinuities. But it is difficult to proof the stability for the whole model including the parameterizations. However, stability has been proven in parts (e.g. the stability of the two-time-level semi-implicit integration scheme for gravity wave motion (Simmons, Temperton, 1996). As the Lax-Richtmyer theorem cannot be applied there is no proof for the convergence of the model equations in the limit of $\Delta t \to 0$. The limitation imposed on Δt by the above theory ensures a bounded error growth in the limit of $\Delta t \to 0$, for the actual Δt used in practice the error growth may still be enormous (Richtmyer, Morton, 1967). For a weather forecaster an accurate solution converges to the veri-

fying analysis. This requires the accurate evolution in time of the initial state. The following analysis examines the sensitivity of the solutions of the SLAVEPP and the CONTROL method to changes in the length of the time-step. Considering the above it is however a reasonable working assumption that the method which has the long time-step solution closer to the short time-step solution, is the better method.

Analysing semi-Lagrangian schemes Lie (Lie, 1998) showed that the implied interpolation of the semi-Lagrangian mechanism may "advect" less accurate results from regions of low regularity (resulting from non-smooth solutions by the physics) into regions with smooth solutions and therefore "pollute" those areas with lower accuracy. In the presented results no evidence could be found for this behaviour. Furthermore, in an operational environment like ECMWF where the same model is run at various resolutions (and thus with various time steps) it is desirable to reduce the "systematic" differences resulting from the use of different time-steps between those solutions. Therefore, the following analysis is regarded as a valid test for the quality of the SLAVEPP scheme.

In order to compare the differences of the CONTROL method and SLAVEPP with regard to their time-step dependence four different 24-hour forecasts using a T_L319 resolution have been run with t=300s and t=3600s time-step, respectively. The accuracy of the CONTROL forecast using the operational configuration is compared with SLAVEPP. As a measure for the deviation of the 3600s-solution from the assumed correct 300s-solution the root mean square error has been computed for both methods using

$$rms = \sqrt{\overline{(F_{t=3600s} - F_{t=300s})^2}}. \qquad (3.1.1)$$

The overbar $\overline{(\ldots)}$ denotes an average over area. The following curves represent area means of forecasts from the 1.08.1998. The values shown in Fig. 3.1-1 are tendencies of various atmospheric parameters. The tendencies are accumulated every time step over a period of 24 hours. Fig. 3.1-1 shows the time evolution of the root mean square error for the two methods for the regions of Europe[Fig. 3.1-1 (a)] and the North Atlantic[Fig. 3.1-1 (b)-(c)] in various model levels. Several areas of the globe in different vertical levels have been compared for the different diabatic and adiabatic tendencies of humidity, temperature, cloud liquid water, cloud fraction and the horizontal wind components. For both methods the solutions with any method especially over land areas (e.g. Europe, North America) are rather strongly time-step dependent. Using SLAVEPP has an overall positive impact on the time-step dependence. The resulting rms errors of method SLAVEPP are smaller or neutral in all levels and all investigated areas. The comparison of the mean error and the root mean square error verified against the CONTROL analysis in the first 24 hours shows that the results of the small time step solutions are very similar using either method. As in Fig. 3.1-2 the t=3600s mean error seems to oscillate around t=300s mean error. The errors for the long time-step solution are also similar between the two methods but the differences are bigger than in the t=300s case. Generally the rms errors seem to be slightly smaller with SLAVEPP verifying over the 24h period. The results are assumed (but due to the expensive computations not proven) to be representative for any date.

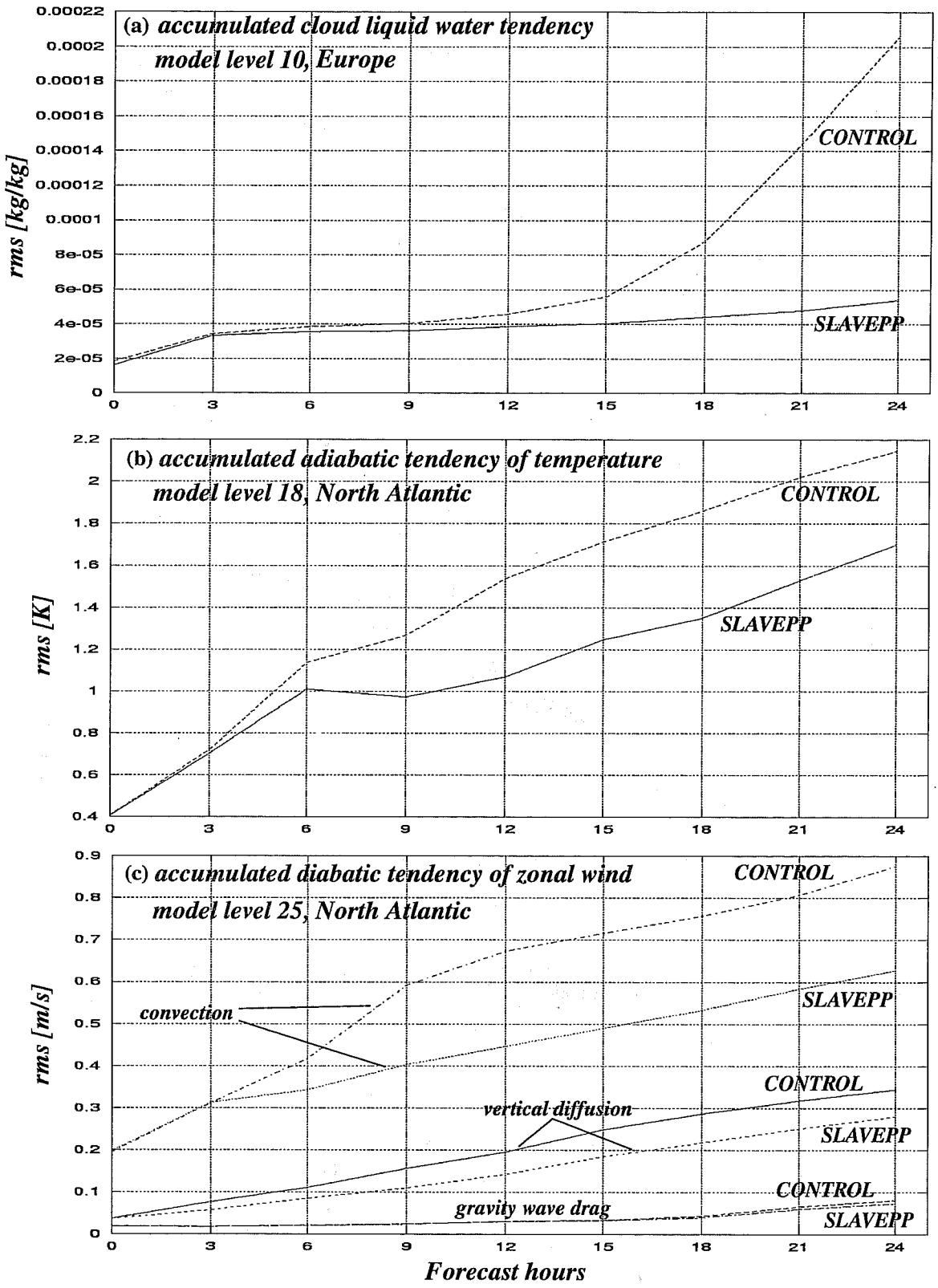

Fig. 3.1-1 Root mean square error as described in equation (3.1.1) of the accumulated diabatic and adiabatic tendencies of temperature, cloud liquid water and the East/West horizontal wind component over a period of 24 hours. The model levels 10,18 and 25 are shown (corresponding approximately to ~200hPa,~500hPa and ~800hPa, respectively). The diabatic tendencies are splitted into the contributing parameterized processes. The values represent area averages over the given area.

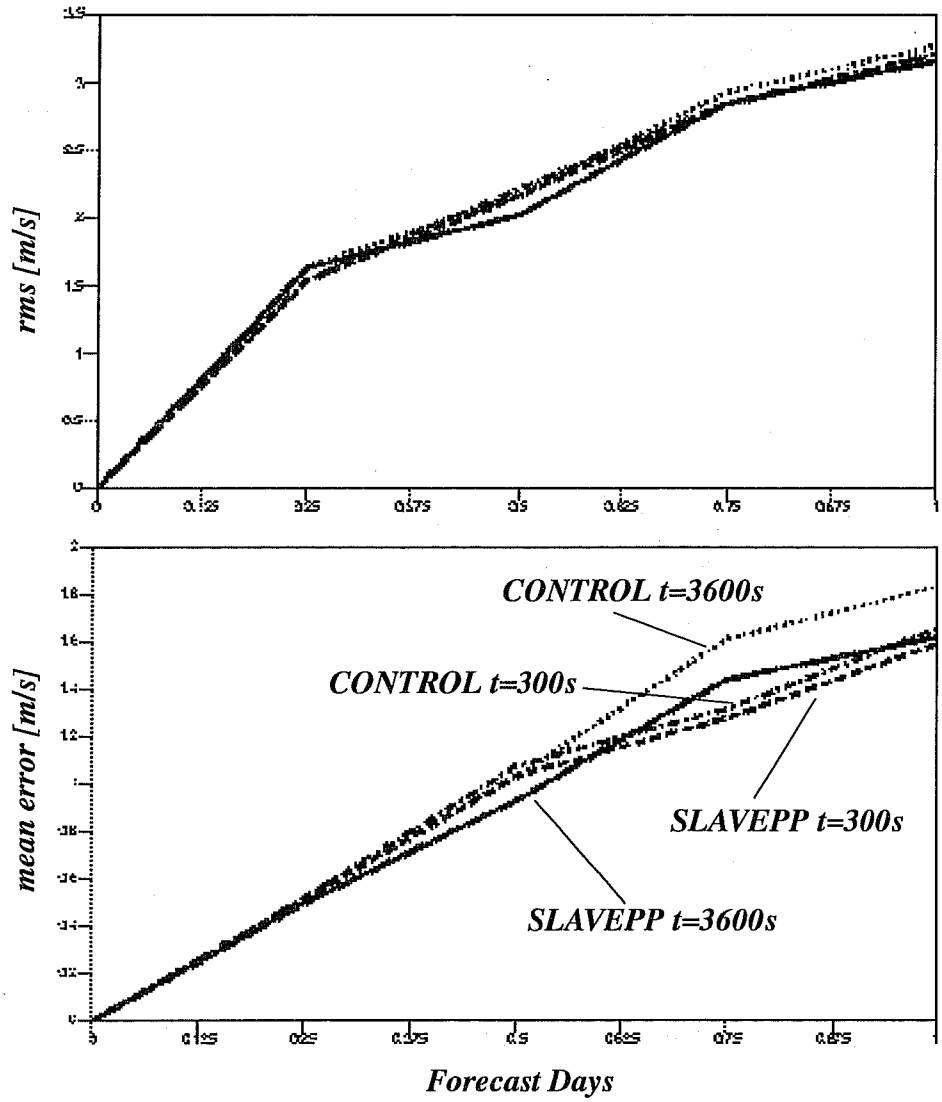

Fig. 3.1-2 Root mean square error and mean forecast error with respect to the analysis for the first 24 hours of the forecast. The vector wind in 850hPa is shown as an area mean for Indonesia. The graphs represent the SLAVEPP scheme and the CONTROL scheme using time steps of t=300s and t=3600s, respectively. The initial date of the forecast is 1.08.1998 12Z.

3.2 Balance between physical parameterizations and the "dynamics"

If equation (2.1.10) would be applied regardless of the nature of the parameterization and their coupling to the "dynamics" the solution can be wrong as shown in Fig. 3.2-1. Comparing the short time-step solution with a longer time-step run huge differences in the wind vectors developed after a six hour forecast especially near orography and in the lowest model level. This is the main reason for the modification described in equation (2.1.17) computing the contributions of vertical diffusion and gravity wave drag only at the arrival point of the trajectory. For these parameterizations it is necessary to use in equation (2.2.3) the same model variable to derive $\tilde{D} = \tilde{D}(F(t))$ and to use as input (e.g. $F(t)$) in order to arrive at the correct equilibrium state between the parameterized vertical massflux of horizontal momentum and the horizontal flux given by the advection. In this case an averaging in time and space using information from the previous time-step may destroy this equilibrium and subsequently lead to wrong results. However, as further tests have shown the gravity wave drag parameterization is not

responsible for this behaviour. The problem is not fully understood and is subject to further investigation.

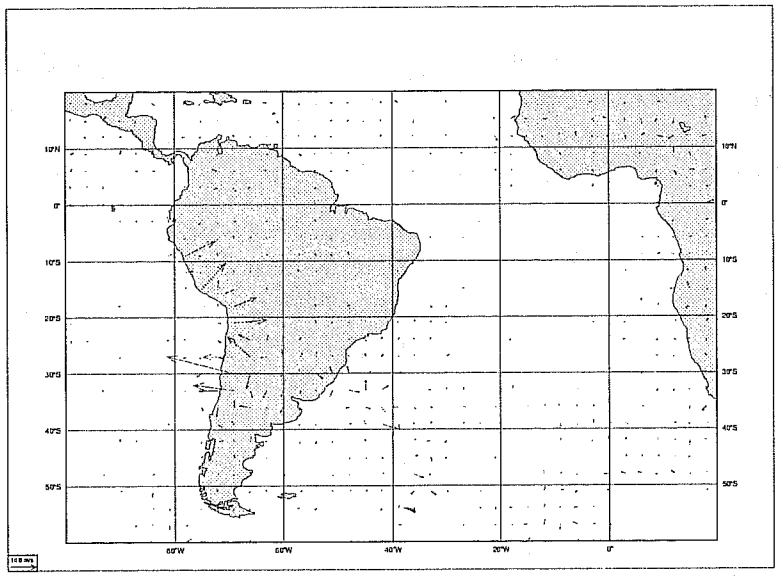

Fig. 3.2-1 The effect of averaging between the endpoints of the semi-Lagrangian trajectory in the lowest model level near high orography. The plot shows the differences in the wind vectors between the t=300s and t=3600s solution if all parameterizations are treated in a "split" way (evaluated half at the arrival point and half at the departure point of the semi-Lagrangian trajectory). The shown differences occurred already after 6 hours in the forecast (08.09.1997) and do not occur if the vertical diffusion parameterization is switched off.

In order to investigate if the model using the SLAVEPP scheme maintains the correct balance between the dynamics and the physical paramterizations the drag coefficient C_D is used (Janssen et. al.(1992), Beljaars (1991)). The drag coefficient describes the drag of the atmosphere against the earth's surface (Stull,1988). It is defined as the relation between the friction velocity u_* representing the surface stress (vertical flux of horizontal momentum) and the mean square wind speed

$$C_D = \frac{u_*^2}{\overline{u^2 + v^2}}. \tag{3.2.1}$$

The solid line shown in Fig. 3.2-2 describes the theoretical value of the drag coefficient in statically neutral conditions and with a logarithmic wind profile. If the wind profile (following Stull,1988) is given as

$$\frac{(\overline{u^2 + v^2})}{u_*} = \frac{1}{k}\ln\left(\frac{z}{z_0}\right) \tag{3.2.2}$$

with the roughness length over the ocean specified by Charnock's relation (Charnock,1955)

$$z_0 = \frac{\alpha}{g}u_*^2 \quad , \tag{3.2.3}$$

the drag coefficient can be derived using equation (3.2.1) by solving the implicit equation

$$C_D = f(C_D) = k^2\left[\ln\left(\frac{zg}{\alpha(\overline{u^2+v^2})C_D}\right)\right]^{-2}. \qquad (3.2.4)$$

It can be seen in Fig. 3.2-2 that both methods maintain the correct balance regardless of the used time step. The large scatter in the plot results from the fact that the assumption of neutral conditions does not strictly hold for each gridpoint of the model in the given area. SLAVEPP seems to represent the theoretical value slightly sharper towards higher wind speeds but cases with particular high wind speeds would have to be run to confirm this impression.

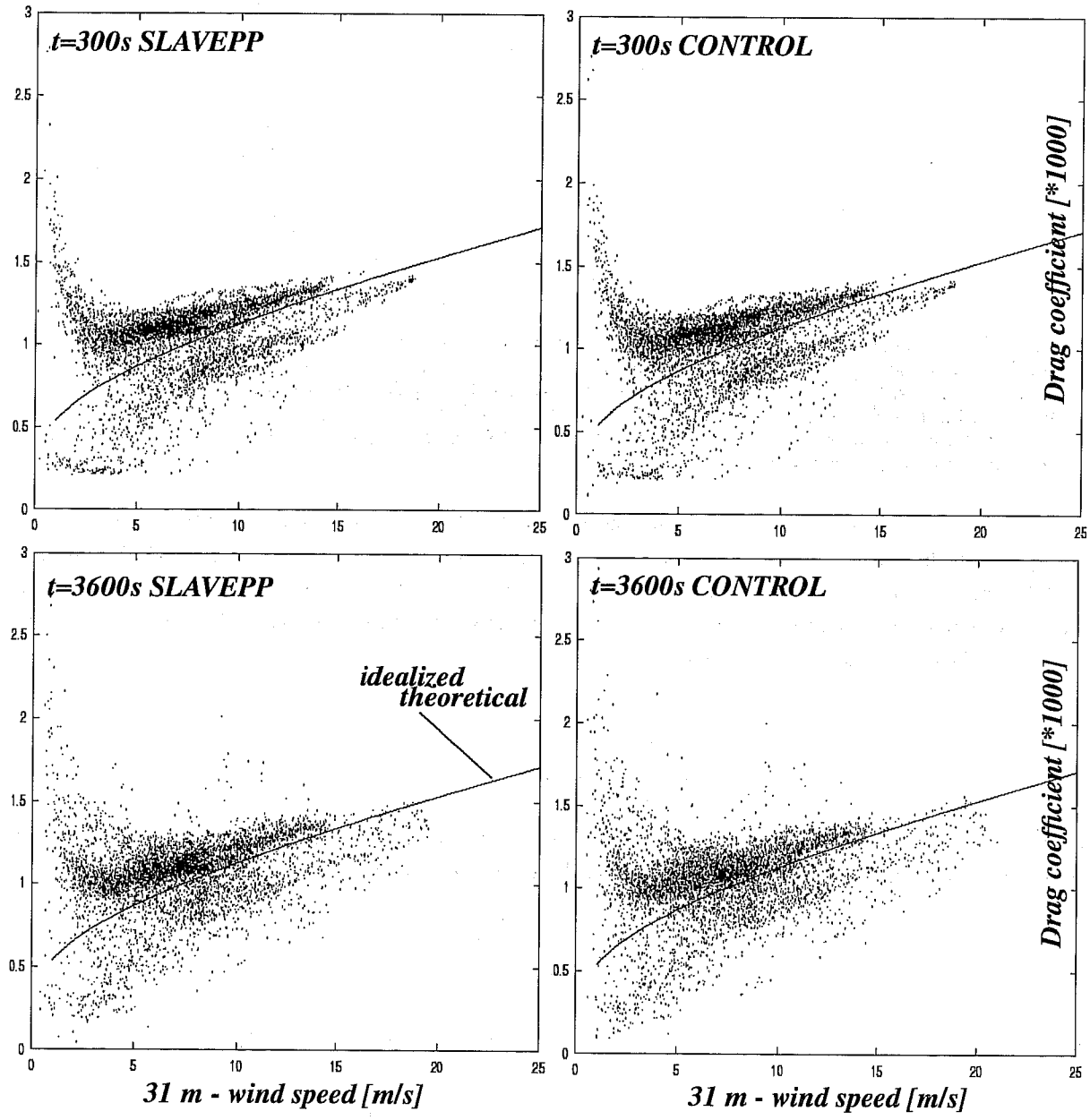

Fig. 3.2-2 Drag coefficient against mean wind speed at the lowest model level (z ≈ 31m) for the SLAVEPP scheme and the CONTROL scheme [using t=3600s and t=300s] for the North Atlantic on the 1.08.1998. The solid line describes the theoretical value of the drag coefficient derived from equation (3.2.4) using $\alpha = 0.018$ and $k = 0.4$.

3.3 Impact on medium range forecasts

In order to assess the impact of SLAVEPP on the medium range analysis and forecast system a data assimilation experiment has been performed in the 4DVar assimilation system with T_L 319 resolution with 31 vertical levels for the period 28 November to 15 December 1997. A series of 10-day forecasts were launched once a day from the 12UTC analyses. Fig. 7.1-2 shows root mean square error and anomaly correlation of the 500hPa height field comparing SLAVEPP with the CONTROL method as a mean over the 18 cases. The time step for all forward model integrations (both methods) has been chosen to t = 1200s. The analyses have been created using the version CY18R5 of the IFS model. Note, that the assimilation using SLAVEPP did not include the modification of cloud liquid water (described in the previous section) but the subsequent forecasts do include the modification. The results shown in Fig. 7.1-2 and in the annex suggest that there is a positive impact in the medium range on the overall forecast skill in both hemispheres. There is a clear benefit towards SLAVEPP visible in all diagrams representing generally lower rms-errors compared to the control forecasts. Investigating the dependence on the time step another set of 14 forecasts has been run using a T_L159 resolution with 31 vertical levels and a T213 resolution with 31 vertical levels. These sets also used an earlier version of SLAVEPP without the described modification of cloud liquid water (IFS version CY16R3). The time step has been chosen as t = 1350s and t = 2700s for the T_L159 cases and t=900s and t=1800s for the T213 cases. In both series (the T_L159 case is shown in Fig. 3.3-1) SLAVEPP is superior to the CONTROL method. It can also be seen that the longer time-step solution is closer to the shorter time-step solution when using SLAVEPP which suggests that the new scheme allows a bigger time-step and subsequently a gain in efficiency. If further tests confirm initial results with an increased time-step from t = 1200s to t = 1800s for the T_L 319 resolution this may result in a gain in efficiency of approximately 30 percent. The T_L 319 resolution is used in the 1998 operational configuration at ECMWF in the 10-day forecast. The T_L159 resolution is used in the ensemble prediction system.

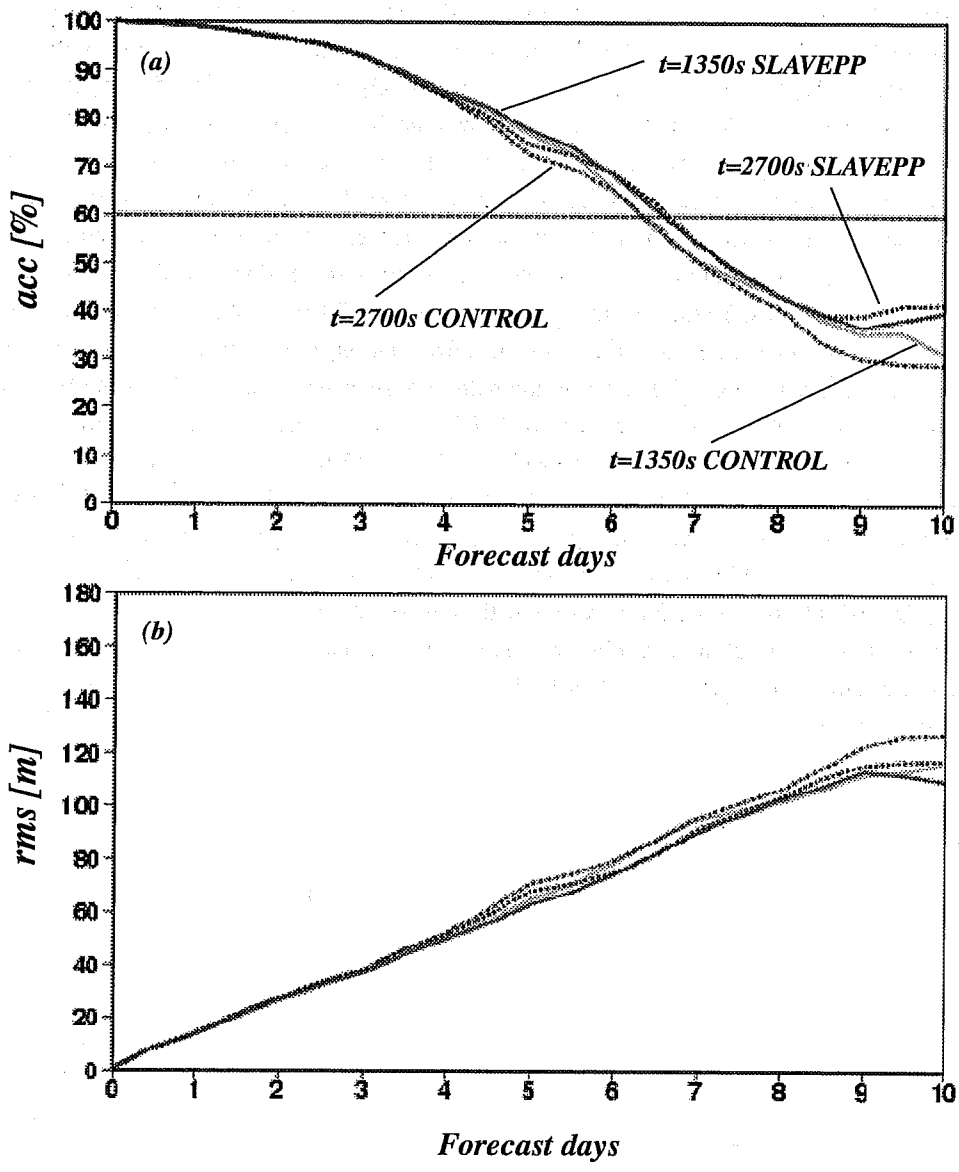

Fig. 3.3-1 Root mean square error (*rms*) (b) and anomaly correlation (*acc*) (a) for Europe. The plots represent a mean over 14 different forecast dates (15th of each month 1996/97) with different time-steps used for the integration. Results are shown for the CONTROL scheme and the SLAVEPP scheme using a T_L159 resolution and 31 vertical levels. The initial data was taken from the operational analysis in both cases.

3.4 Coupling to the wave model

In the framework of SLAVEPP it has been tried to utilize the predictor values of the wind model variables rather then the surface winds at time step t as input to the coupled wave model. This produces a more balanced coupling of the diagnostic fields from the atmospheric part and the wave model part as the best available first guess of the wind fields is provided to the wave model. In order to investigate the influence of the revised coupling to the wave model the standard deviation and anomaly correlation for wave height and 10-meter wind speed are plotted and compared to the CONTROL method. Fig. 3.3-5 indicates a slightly positive impact comparing the to schemes.

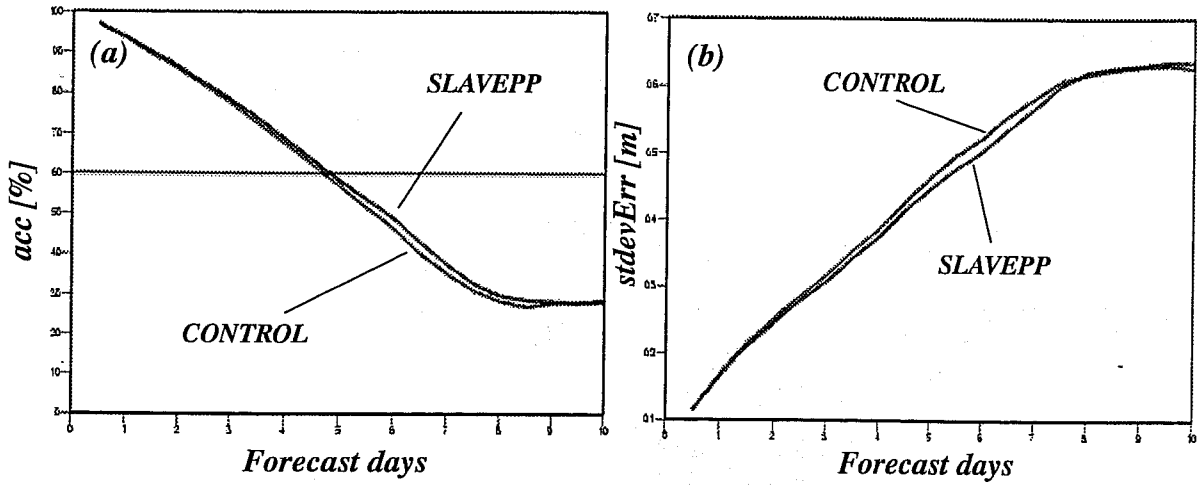

Fig. 3.4-1 (a) Anomaly correlation (acc) and (b) standard deviation of error (stdevErr) for wave heights as a mean over 21 cases for the Northern Hemisphere. Both schemes used a two-way coupling to the wave model. The forecasts used a T_L319 resolution with 31 vertical levels.

3.5 Comparison of total rainfall against observations

The areas of East Asia and Europe have been examined comparing the total rainfall after 48 hours with the available observations. Fig. 7.1-12 compares the results using the CONTROL scheme and the SLAVEPP scheme for the area of East Asia. Fig. 7.1-13 shows the mean forecast error of the operational forecast from 4/07/1998 compared to the observations. Fig. 7.1-14 shows the mean forecast error using the SLAVEPP scheme compared to the observations. The small numbers represent the observations with the contours and the big numbers representing the model results. There is some evidence of overestimating the actual observed rainfall in some parts of the forecast. This overestimation of the total rainfall in the CONTROL method is reduced by method SLAVEPP in both cases. It is interesting to note that there is not only a general reduction of rainfall compared to the CONTROL scheme, which may have been expected from the "smoothing" effect of averaging, but in some cases there is a better positioning of the forecasted rainfall maxima compared to the observations. This can be seen for example in the relative maximum of rainfall in the top left of Fig. 7.1-13 and Fig. 7.1-14 . The positive result seems to be reflected in the comparisons of precipitation regarding the model climate (see section 3.8). However, only few cases are presented and this is not enough to draw general conclusions about the performance of the SLAVEPP scheme with regard to an improvement of the overall rainfall forecast. Nevertheless, the presented cases stress the fact that there is no evidence of any "smoothing" of sharp discontinuities if SLAVEPP is used instead of the CONTROL method.

3.6 Numerical "noise"

"Although the semi-Lagrangian semi-implicit discretization (SLSI) of the primitive meteorological equations has resulted in significant savings of CPU, achieving its full potential has been hampered by the intermittent appearance of non-meteorological oscillations; 'noise'" (McDonald, 1998). In his catalogue of sources for this "noise" McDonald referred to the coupling of the "dynamics" to the "physics" and the parameterizations to each other as two possible sources.

Numerical "noise" that appeared in the level 9 temperature field of the operational forecast of the 4.01.1997 lead to a reduction of the operationally used time-step in the two-time level advection scheme (Temperton, 1997). Noise may occur due to the inaccuracy, instability or oscillating behaviour of the numerical schemes. The noise shown in

Fig. 3.6-1 (c) can be almost eliminated by choosing half the time-step (Fig. 3.6-1 (d)) or as shown by Hortal (1998) using a revised Stable Extrapolating Two Time Level Scheme (SETTLS). However, using SLAVEPP in the forecast and in the data assimilation that derives the analysis field for the forecast a smooth field is obtained without compromising on the time-step. The general flow pattern compared to the analysis of the 9.01.1997 Fig. 3.6-2 identifies the forecasts shown in Fig. 3.6-1 (a) and (b) as the more accurate solution with regard to this analysis.

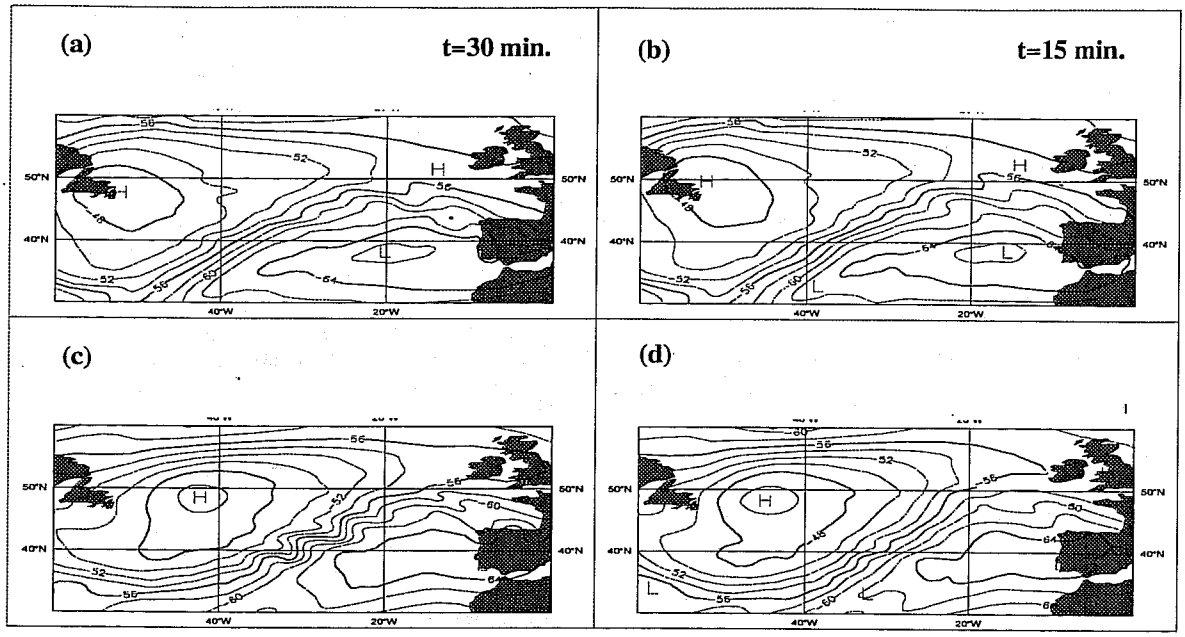

Fig. 3.6-1 Noise as seen in the operational 5-day T213 forecast from 01.01.1997(+120h) [(c) time step t=1800s and (d) time step t=900s] compared to the results achieved using the SLAVEPP scheme [(a) time step t=1800s and (b) time step t=900s].

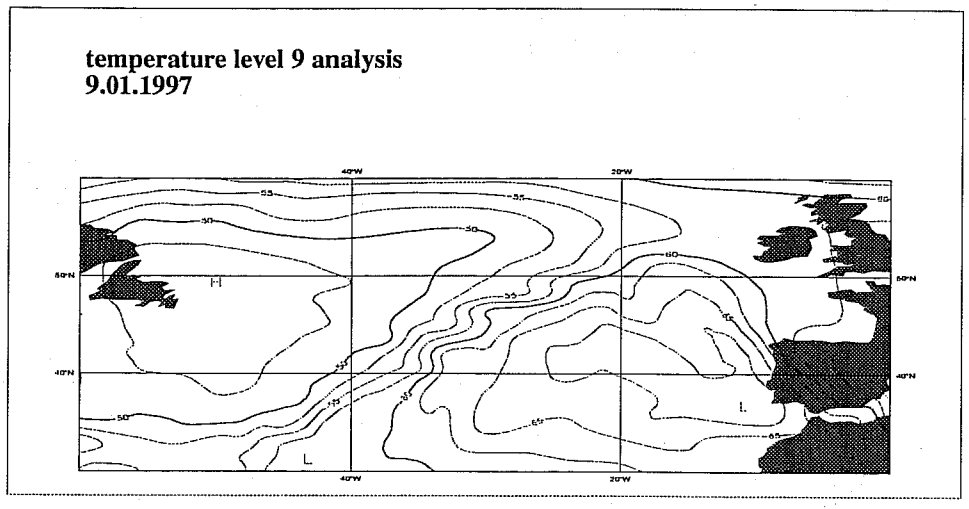

Fig. 3.6-2 Model level 9 temperature analysis of the 9.01.1997. The analysis field shows already some noise. The position of the high pressure centre and the flow pattern (e.g. north-west of Spain) corresponds to the situation found in Fig. 3.6-1 (a) and (b).

3.7 The Tropical storm Erika

The hurricane Erika was first tracked as a hurricane on 4 September 1997 in the Caribbean. The hurricane passed about 300 nautical miles east of Bermuda on the 10th and became embedded in westerly steering currents which caused a turn toward the east-northeast on the 11th and 12th. By this time, weakening had commenced due to a combination of cool sea surface temperatures and westerly winds aloft. Winds dropped below hurricane force on the 12th. However, Erika periodically retained deep convection near its centre for another four days along with wind speeds between 45 and 60 knots while it moved mostly eastward across the North Atlantic. The centre passed very near the western-most Azores on the 15th and tropical storm conditions were experienced in these islands. Erika then lost most of its deep convection and became extratropical by the 16th. It continued moving northeastward for several more days, followed by dissipation on the 20th while located about 200 nautical miles southwest of Ireland. The information has been largely taken from the archive of the National Hurricane Centre (NCEP, Lawrence, 1997). The last few days of this storm have been compared with medium range results of the IFS model using SLAVEPP and the CONTROL method. A high resolution with a spectral truncation of T_L639 with 31 levels has been chosen and tested with a slightly bigger time step t=900s (as compared to the default t=600s normally used in this resolution). Fig. 3.7-1 shows a more realistic representation of the geographical position of the storm using SLAVEPP if compared to the CONTROL method. This gives another indication of the benefit of the SLAVEPP scheme if the time step is increased in order to gain efficiency with less loss of accuracy when moving to higher resolutions.

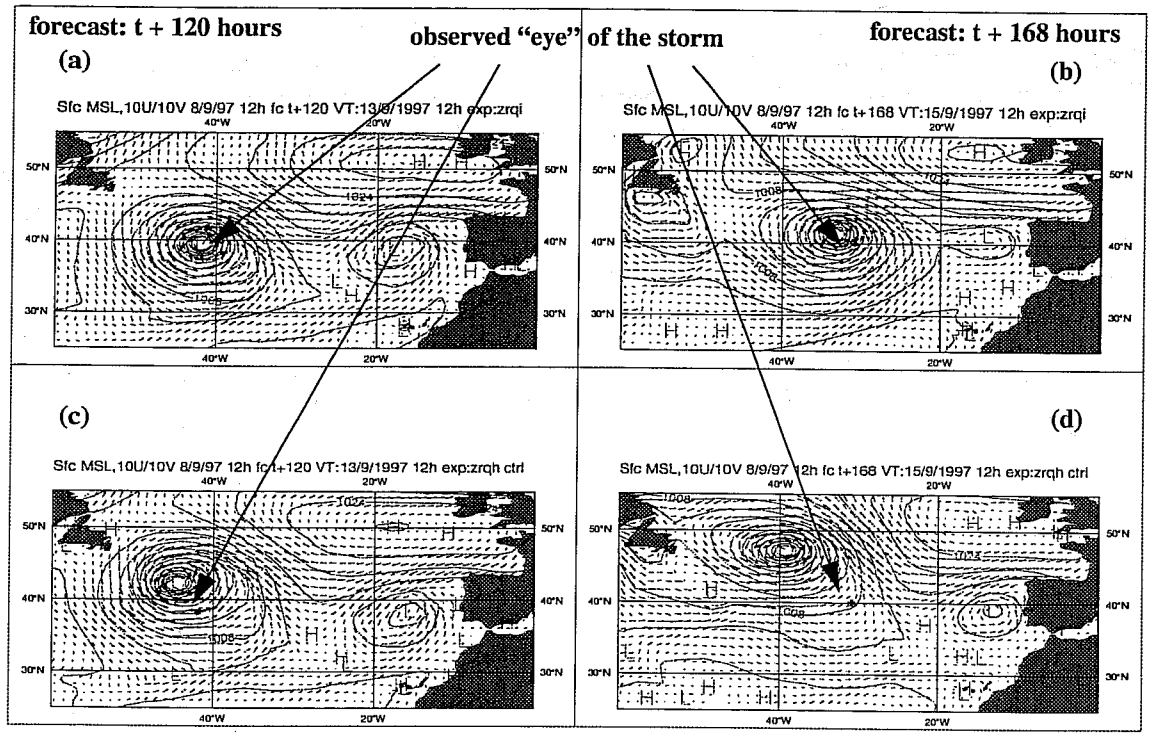

Fig. 3.7-1 : Evolution of the tropical storm Erika over the North Atlantic using a T_L639 truncation with 31 vertical levels. (a) and (b) show the results of the SLAVEPP scheme whereas (c) and (d) represent the CONTROL forecast. Both forecasts use a time-step of 15 minutes. The * denotes the observed centre of pressure as given by the reports issued from the National Hurricane Centre (NCEP) [13.09.97 09.00/ 15.00: 1000hPa; 15.09.97 09.00: 994hPa, 15.00: 997hPa]. Note, that the forecasted winds are very strong and the forecasted centre pressure is too deep in both cases.

3.8 Impact on model "climate"

In order to make a preliminary assessment of the impact upon the seasonal climatology of the model, two simulations using a T63 resolution with 31 vertical levels have been run with the SLAVEPP scheme and the CONTROL scheme. The period is chosen to cover both a northern hemispheric summer (June/July/August) and winter (December/January/February) with the initial data given by the ECMWF re-analysis project (ERA). The start date was chosen a month earlier than the actual verifying period of three months. Zonally averaged mean values of temperature, mass flux, vertical velocity and the horizontal wind components are compared to the ERA analysis for both methods (shown is temperature in Fig. 7.1-4). As a verification for the cloud parameters the global distribution of mean cloud cover given by the International Satellite Cloud Climatology Project (ISCCP) (see Rossow and Schiffer (1991)) is used. The estimated precipitation from the dataset of the Global Precipitation Climatology Project (GPCP) is used to compare the different precipitation patterns (Fig. 7.1-5 and Fig. 7.1-6). Outgoing longwave radiation (OLR) and top short wave radiation (TSR) at the top of the atmosphere are compared to the measured/estimated Earth Radiation Budget Experiment (ERBE) dataset. In general the differences are rather small between the two methods. Increased cloud cover can be seen in the upper troposphere in the tropics. This is confirmed in a model level cross section comparison of zonally averaged values of cloud fraction and cloud liquid water. The slight increase in high clouds in the tropics compares slightly worse to the ISCCP data in the northern hemispheric summer case and neutral or slightly better in the winter case. There is an improvement in summer comparing the cloud cover against ISCCP in the subtropics. The bias over Australia is completely removed which seems to be also beneficial for the radiation budget at the top of the atmosphere compared to ERBE. It is interesting to note, that the change in the treatment of the cloud liquid water and ice does not effect the model climate other than described. The precipitation compared to GPCP (Fig. 7.1-5 and Fig. 7.1-6) seems to better represented when using SLAVEPP in the summer case and appears neutral in the winter case. The biggest differences can be identified in the East Asian region and over Europe. These areas have been investigated further in case studies of short range forecasts compared to observations. The differences in the surface fluxes amount to a net difference of less than 1 Watt/m^2. There is generally slightly less radiation reaching the surface and a slightly increased latent heat flux in various areas. The zonal mean values of temperature compared to the ERA analysis show a slightly reduced positive bias in the upper troposphere of the tropics and a reduction of the negative biases by two degrees towards the mid-latitudes and poles in the northern hemispheric winter case (Fig. 7.1-4). The summer case is rather neutral. The strength of the subtropical jetstreams seems to be slightly improved with the SLAVEPP scheme compared to ERA. The impact on humidity, mass flux and vertical velocity is not significantly different between the two schemes.

The most noticeable impact is seen in the mass conservation. The mass conservation is given by the continuity equation which in integrated form gives an equation for the rate of change of the surface pressure. The global mass is therefore often expressed in units of pressure. Here the residuum of the initial mass minus the final mass after every 24 hours has been computed. Fig. 3.8-1 shows the time series of this residuum expressed in Pascal for the northern hemispheric summer case. The residuum of the run using the SLAVEPP scheme meanders around zero with 3-4 Pascal deviation. The CONTROL method reaches a deviation of 17 Pascal at the end of the three month period indicating a far worse conserving behaviour. The results are confirmed in the northern hemispheric winter case resulting in a 12 Pascal deviation difference between the SLAVEPP scheme and the CONTROL scheme.

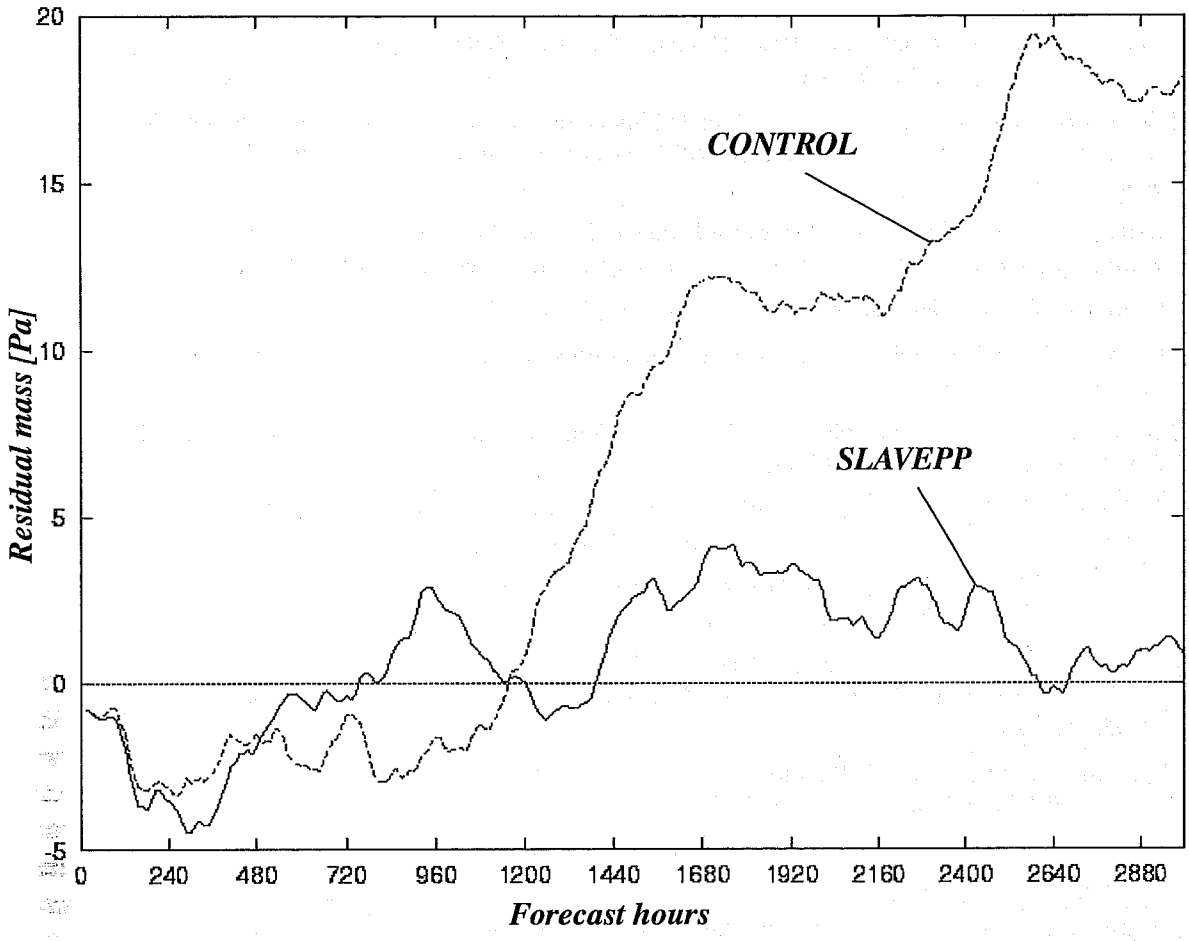

Fig. 3.8-1 Mass conservation: The residuum of the initial mass minus the final mass after every 24 hours is shown as a time series for the northern hemispheric summer case (June/July/August). After the three month forecast integration a difference of 15 Pascal has developed between the two schemes.

4.0 Concluding remarks

The revised coupling of the physical parameterizations to the "dynamic" model equations called SLAVEPP leads to more stable and more accurate results. The comprehensive comparisons using various measures show that there is an improvement in the overall forecast skill. Numerical noise is reduced. There may be the possibility to increase the time-step and therefore gain efficiency. However, it should be noted, that there is also a loss of forecast skill between the short and the longer time-step solution with the revised scheme even though the overall "scores" are better than the control in both cases. The SLAVEPP scheme conserves the total mass better than the CONTROL scheme.

The currently described method may only be regarded as a first step towards an enhanced numerical treatment of the physical parameterizations. A better coupling of the parameterizations with the "dynamics" may be achieved by solving the semi-implicit parameterized contributions together with the semi-implicit corrections of the adiabatic part. It is not clear if this will have an impact on the model performance and therefore justifies the likely increase in computational effort. Furthermore, a review of the numerical schemes inside the physics with regard to numerical stability and accuracy and their applicability to high resolution modelling with reasonably large time steps is needed to prepare for the future resolutions used in medium range weather prediction.

5.0 References

[1] Barkstrom,B.R. and Smith, G.L., 1986: The Earth Radiation Budget Experiment: Science and Implementation, *J. Geophys. Res.*, **24**, 379-390.

[2] Bates, J.R., 1995: Recent Forecast and Climate Simulation Experiments with a Global Finite Difference Semi-Lagrangian Model, *Proceedings of the ECMWF Seminar on Semi-Lagrangian methods, Reading United Kingdom, ECMWF*, 155-165.

[3] Beljaars, A., 1991: Numerical Schemes for Parameterizations, *Proceedings of the ECMWF Seminar on Numerical Methods in Atmospheric Models, Reading United Kingdom, ECMWF*, 1-42.

[4] Charnock, H., 1955: Wind stress on a water surface, *Q. J. Royal Meteorol. Soc.*, **81**, 639-640.

[5] Geleyn, J.F., 1998: Stability of a coupled advection-diffusion equation as used in the IFS, *personal communications.*

[6] Grabowski, W.W., Smolarkiewicz, P.K., 1996: Two-Time-Level Semi-Lagrangian Modelling of Precipitating Clouds, *Mon. Wea. Rev.*, **124**, 487-497.

[7] Hortal, M., 1991: Formulation of the ECMWF model, *Proceedings of the ECMWF Seminar on Numerical Methods in Atmospheric Models, Reading United Kingdom, ECMWF*, 261-280.

[8] Hortal, M., 1998: New two-time-level Semi-Lagrangian Scheme, *Research Department Memorandum at ECMWF*, R60.5/MH/12, obtainable from M. Hortal, ECMWF.

[9] Huffman, G.J., Adler, R.F., Arkin, P., Chang, A., Ferraro, R., Gruber, A., Janowia, J., McNab, A., Rudolf, B., Scneider, U., 1997: The Global precipitation Climatology Project (GPCP) combined precipitation dataset. *BAMS*, **78**, 5-20.

[10]Janssen, P., Beljaars, A.C.M., Simmons, A., Viterbo, P., The Determination of the Surface Stress in an Atmospheric Model, *Mon. Wea. Rev.*, **120**, 2977-2985.

[11]Lie, I., 1998: On the Stability and Accuracy of Semi-Lagrangian Schemes, *Research Report, DNMI No.***72**, *ISSN* 0332-9879.

[12]McDonald, A., Haugen, J., 1992: A two-time-level, three dimensional, semi-Lagrangian, semi-implicit, limited area, gridpoint model of the primitive equations, *Mon. Wea. Rev.*, **120**, 2603-2621.

[13]McDonald,A., 1998: The Origin of Noise in Semi-Lagrangian Integrations.*Proceedings of the ECMWF Seminar on Recent Developments in Numerical Methods for Atmospheric Modelling, Reading United Kingdom, ECMWF*, to be published.

[14]Moorthi, S., Higgins, R.W., Bates, J.R., 1995: A Global Multilevel Atmospheric Model Using a Vector Semi-Lagrangian Finite-Difference Scheme. Part II: Version with Physics, *Mon. Wea. Rev.*, **123**, 1523-1541.

[15]Nieminen, R. 1983: Operational verification of ECMWF forecast fields and results for 1980-1981, *ECMWF Tech. Rep.*, **36**, 8pp.

[16]Oriol, E., 1982: Energy budget calculations at ECMWF, *ECMWF Tech. Rep., 35*, 9pp.

[17]Rossow, W.B. and Schiffer, R.A., 1991: ISCCP cloud data products, *BAMS*, **72**, 2-20.

[18]Richtmyer and Morton, 1967: Difference Methods for Initial-Value Problems, *John Wiley & Sons, New York, London, Sydney, 45pp.*

[19]Simmons, A. and Temperton, C.: Stability of a two-time-level semi-implicit integration scheme for gravity-wave motion, *ECMWF Tech. Rep., 226.*

[20]Simmons, A. J., 1995: The Skill of 500hPa Height Forecasts, *Proceedings of the ECMWF Seminar on Predictability, Reading United Kingdom, ECMWF*, 19-68.

[21]Staniforth, A., Coté, J., 1991: Semi-Lagrangian Integration Schemes for Atmospheric Models - A Review, *Mon. Wea. Rev.*, **119**, 2206-2223.

[22]Stull, R. B., 1988: An Introduction to Boundary Layer Meteorology, *Kluwer Academic Publishers, Dordrecht, Boston, London, 67pp.*

[23]Temperton, C., 1997: Reduction of the model time step, *Research Department Memorandum at ECMWF,* R60.6.1/CT/6/NA, obtainable from C. Temperton, ECMWF

[24]Williamsen D.L., Olsen, J.G., 1994: Climate Simulations with a Semi-Lagrangian Version of the NCAR Community Climate Model, *Mon. Wea. Rev.*, **122**, 1594-1610.

6.0 Acknowledgements

I am grateful to M. Hortal for his scientific advice during the implementation of the revised scheme. I would like to thank J.-F. Geleyn for suggesting and discussing the simplified stability analysis. Furthermore, I would like to thank A. Beljaars, C. Jakob, J. Teixera and P. Janssen for useful discussions during the early stages of the development. Suggestions by M. Miller, A. Beljaars, M. Cullen and M. Hortal greatly improved the first version of the paper. I am grateful to A. Hollingsworth for his comprehensive analysis and criticism of an earlier version of the manuscript.

7.0 Appendix

7.1 Figures

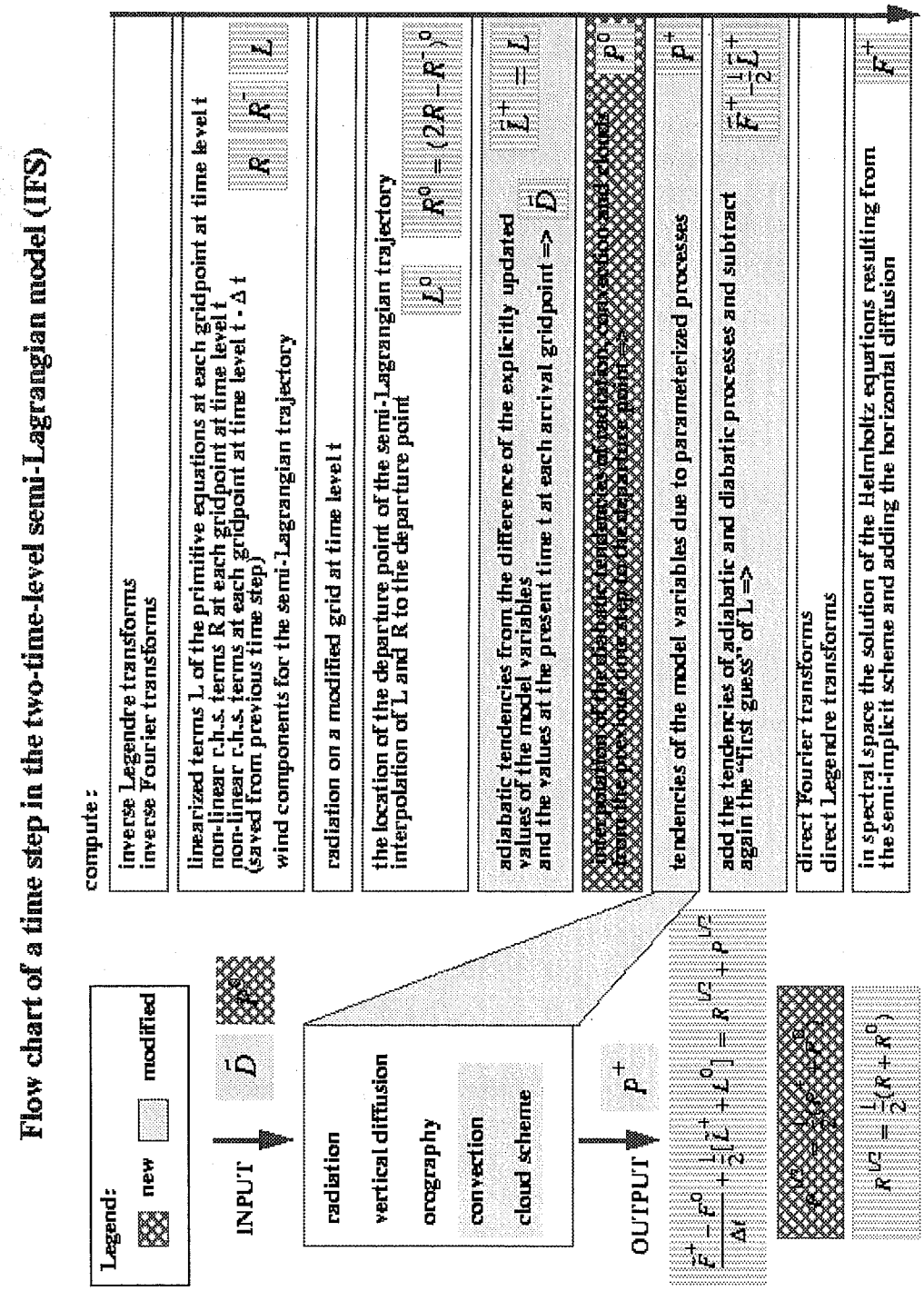

Fig. 7.1-1 A typical time-step in the two-time level semi-Lagrangian version of the IFS model highlighting graphically the proposed changes to the current operational configuration.

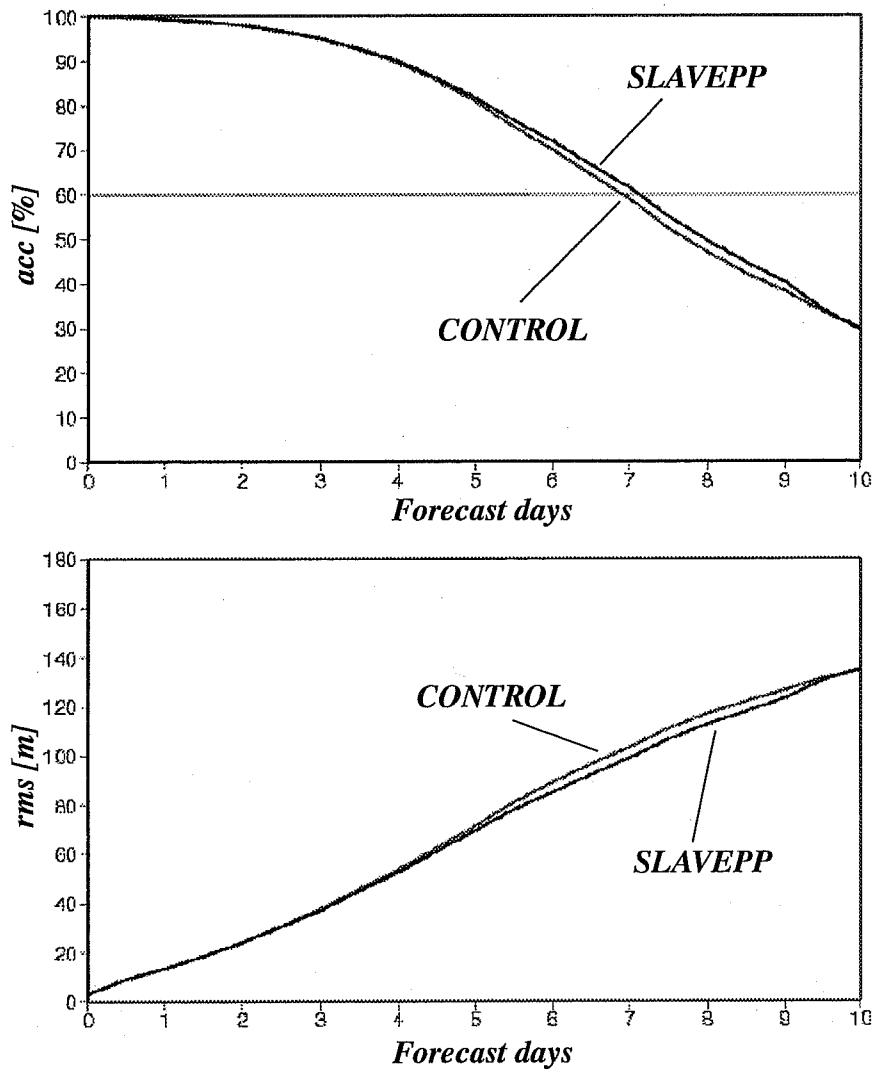

Fig. 7.1-2 Root mean square error (*rms*) and anomaly correlation (*acc*) for the Northern Hemisphere. The graphs represent an area mean over 18 forecasts (28.11.1997 - 15.12.1997 12Z). The forecasts use a T_L319 resolution with 31 vertical levels. The time step for both schemes was t=1200s. The SLAVEPP scheme shows smaller rms and higher anomaly correlation compared to the CONTROL.

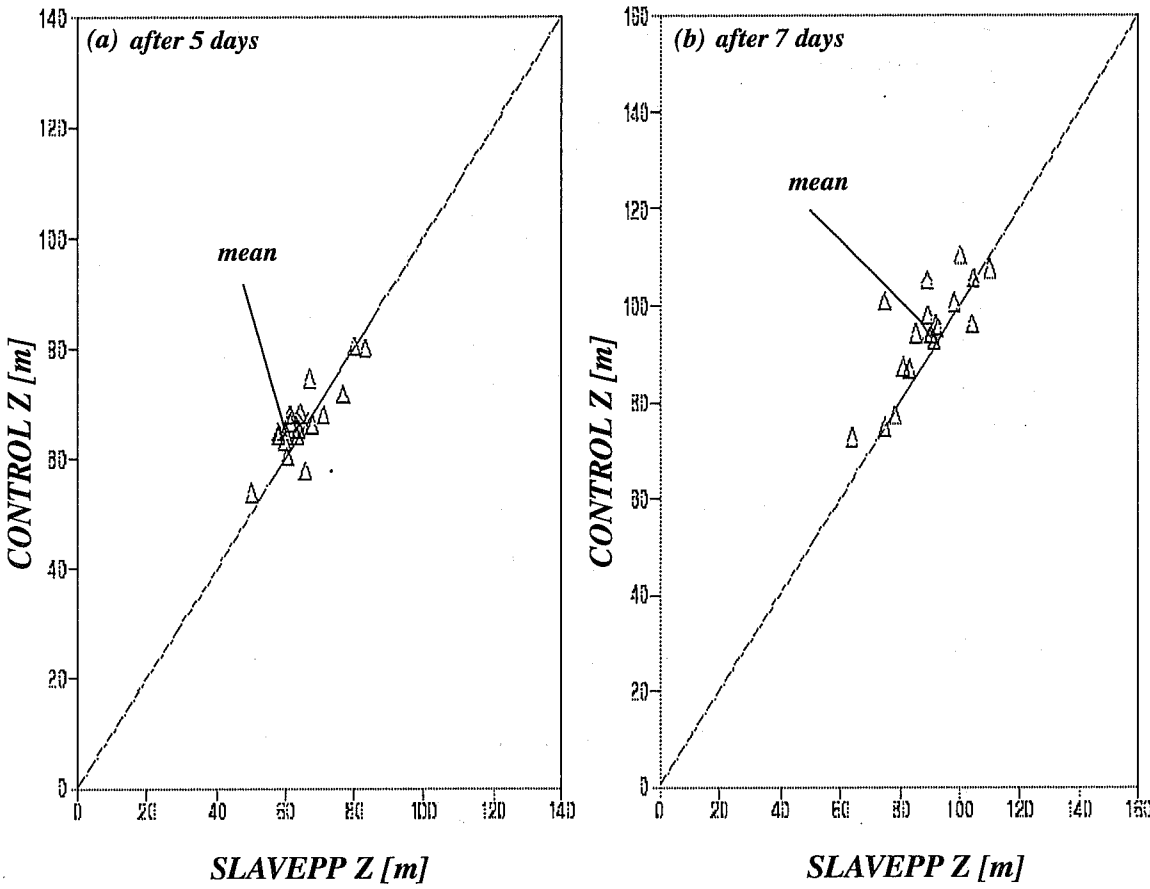

Fig. 7.1-3 Scatter plot for the SLAVEPP scheme and the CONTROL scheme. The points in the diagram represent the root mean square error of the 500hPa geopotential height (Z) field of all 18 forecasts starting on 28.11.1997. Points on the solid line represent cases with equal error in both methods. The forecasts after (a) five days and after (b) seven days are shown. The values represent area means averaged over the Southern Hemisphere. The cross marks the mean of the 18 cases.

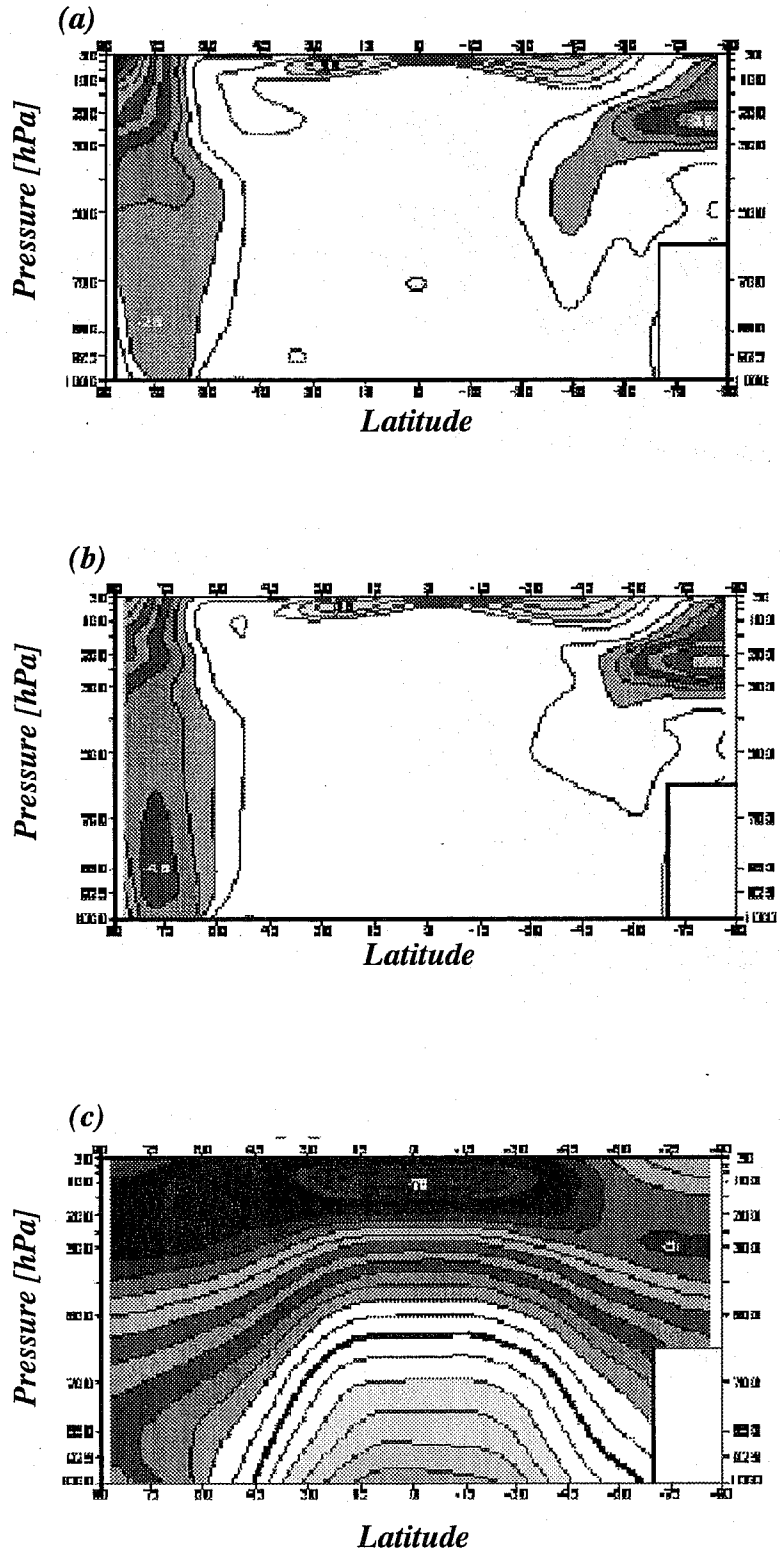

Fig. 7.1-4 Zonal mean cross section of temperature comparing (a) the difference of the SLAVEPP scheme against the re-analysis (ERA) and (b) the difference of the CONTROL scheme against ERA. (c) shows the ERA analysed temperature field for the three month period (December/January/February, 1987). Contours are in (a),(b) 1K and (c) 5K intervals.

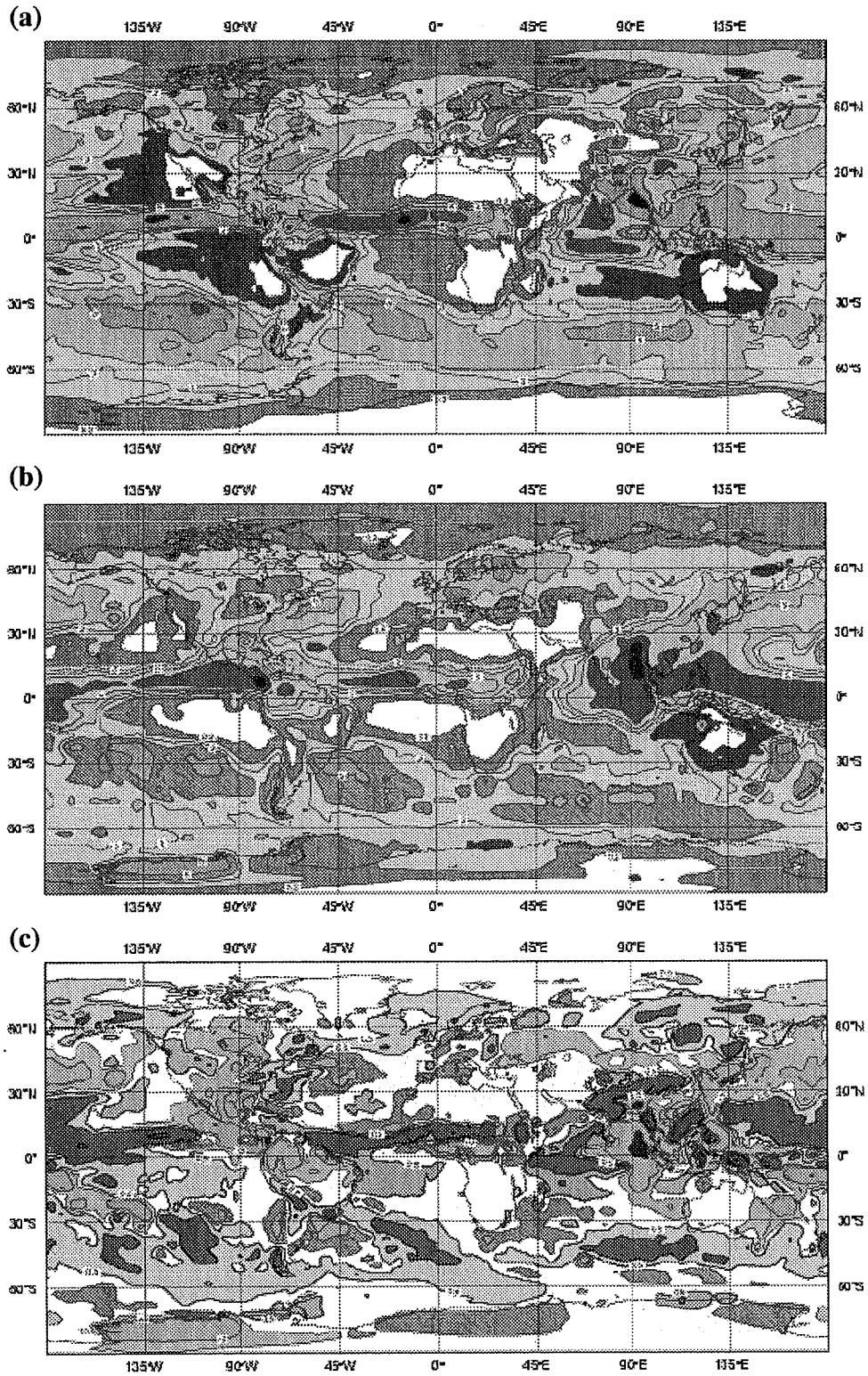

Fig. 7.1-5 (a) shows the total precipitation [mm/day] using the SLAVEPP scheme. (b) shows the estimated precipitation from the dataset of the Global Precipitation Climatology Project (GPCP). (c) shows the differences of the two global datasets. The data covers the three month period (June/July/ August, 1987).

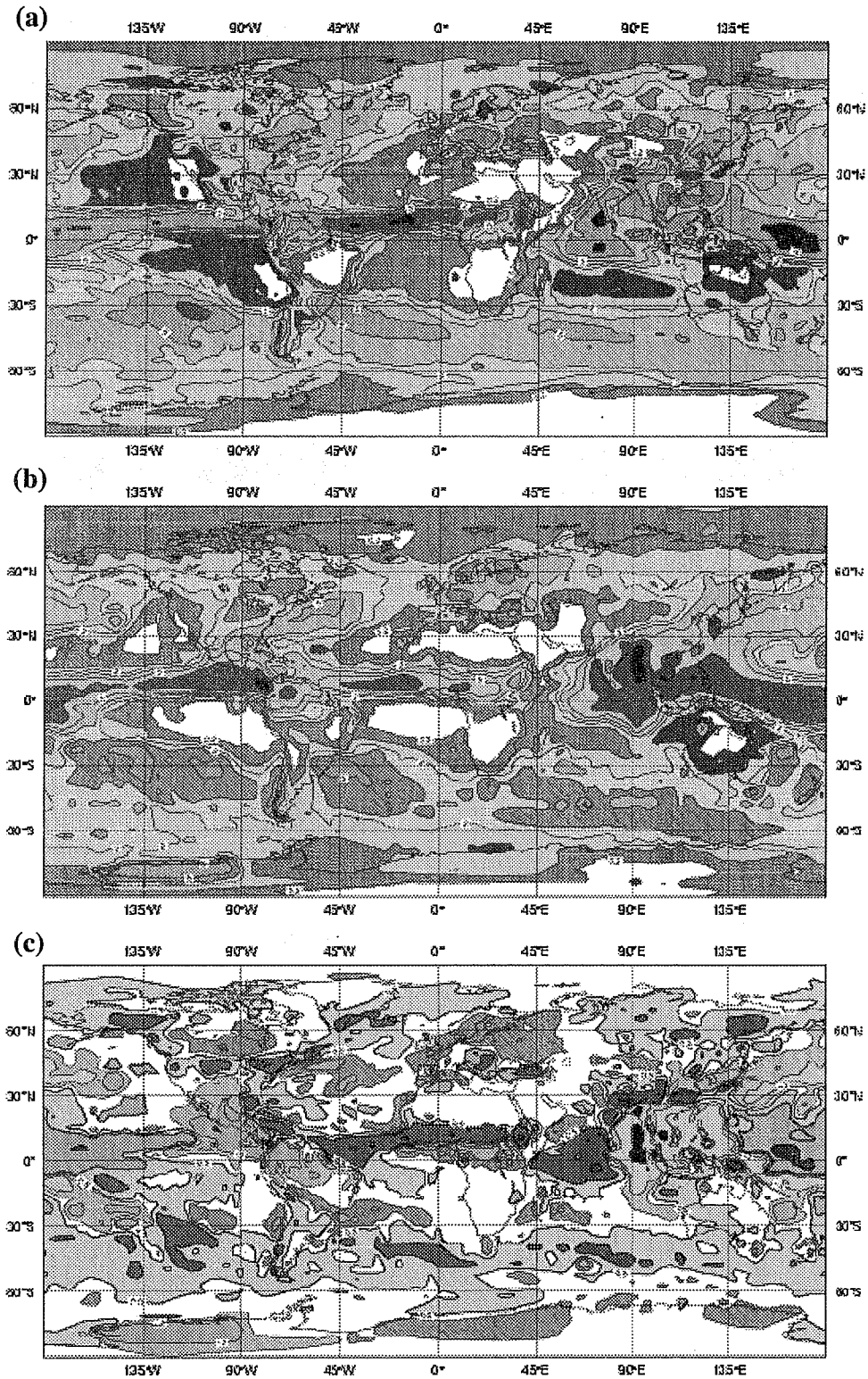

Fig. 7.1-6 (a) shows the total precipitation [mm/day] using the CONTROL scheme. (b) shows the estimated precipitation from the dataset of the Global Precipitation Climatology Project (GPCP). (c) shows the differences of the two global datasets. The data covers the three month period (June/July/ August, 1987).

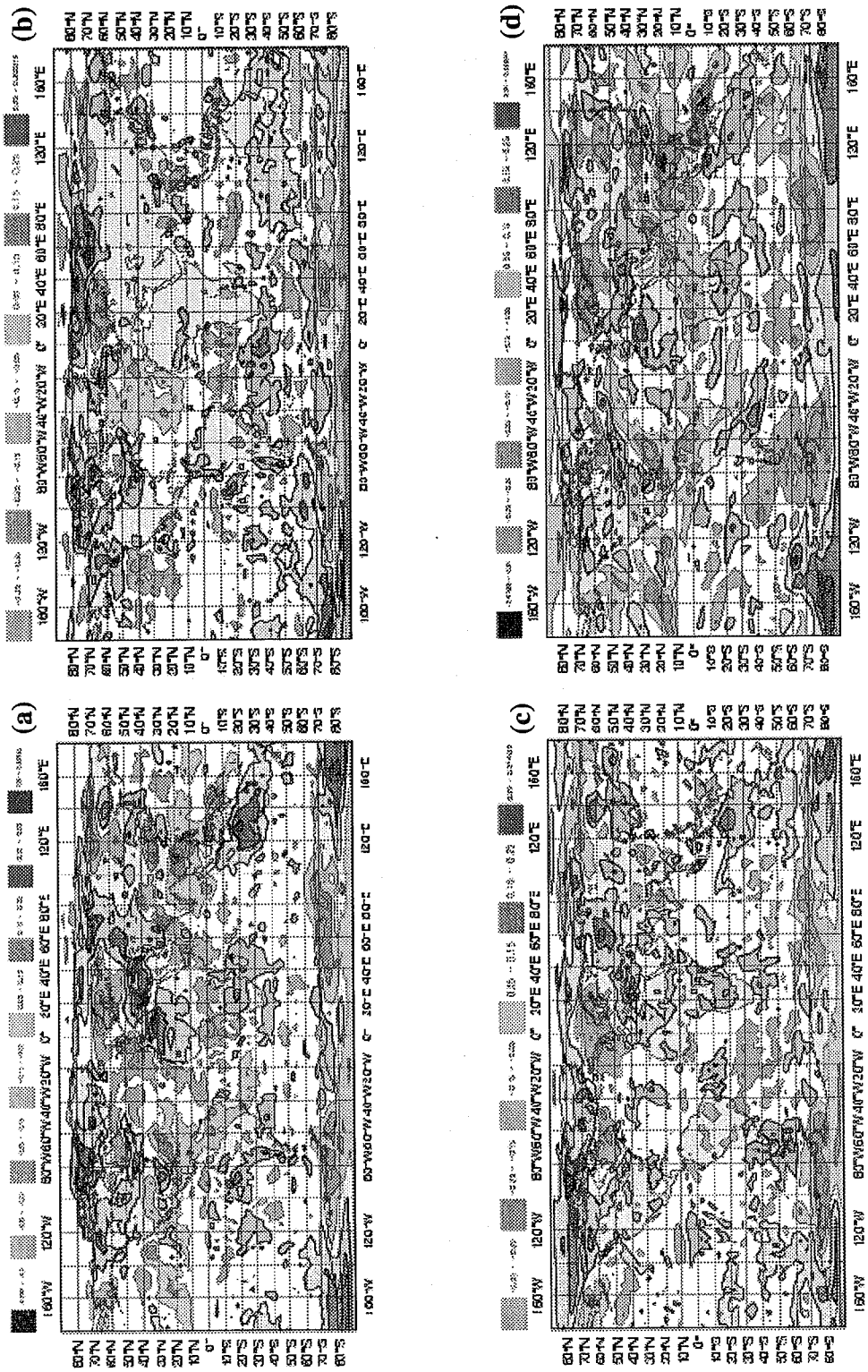

Fig. 7.1-7 shows the difference CONTROL minus SLAVEPP scheme for the parameters (a) total cloud cover [%], (b) low, (c) medium and (d) high cloud cover [%]. The data covers the three month period (June/July/August, 1987). The differences are small and accumulate to 1%-2% in the global mean.

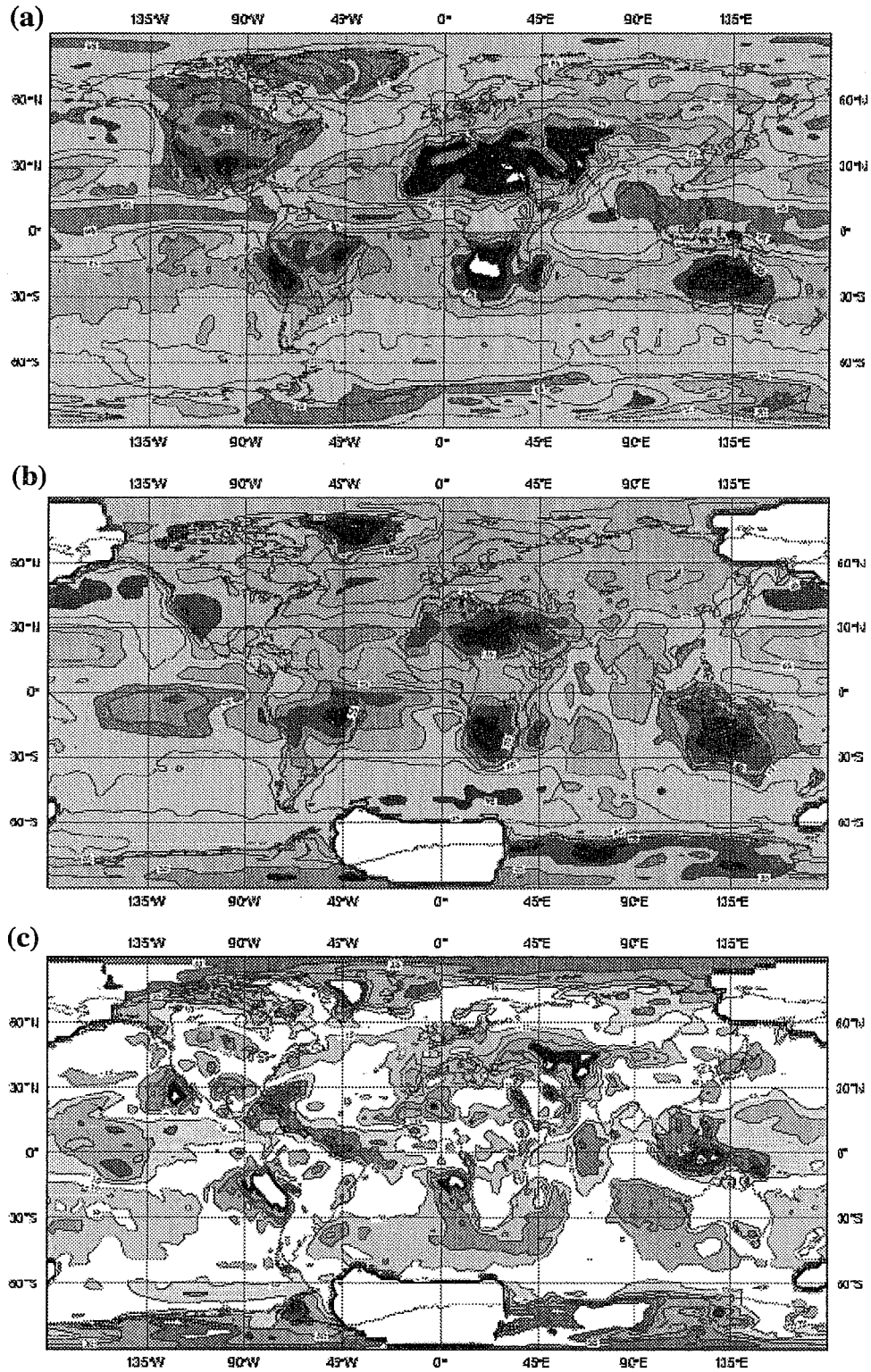

Fig. 7.1-8 (a) shows the total cloud cover [%] using the SLAVEPP scheme. (b) shows the estimated cloud cover given by the International Satellite Cloud Climatology Project (ISCCP). (c) shows the differences of the two global datasets. The data covers the three month period (June/July/August, 1987).

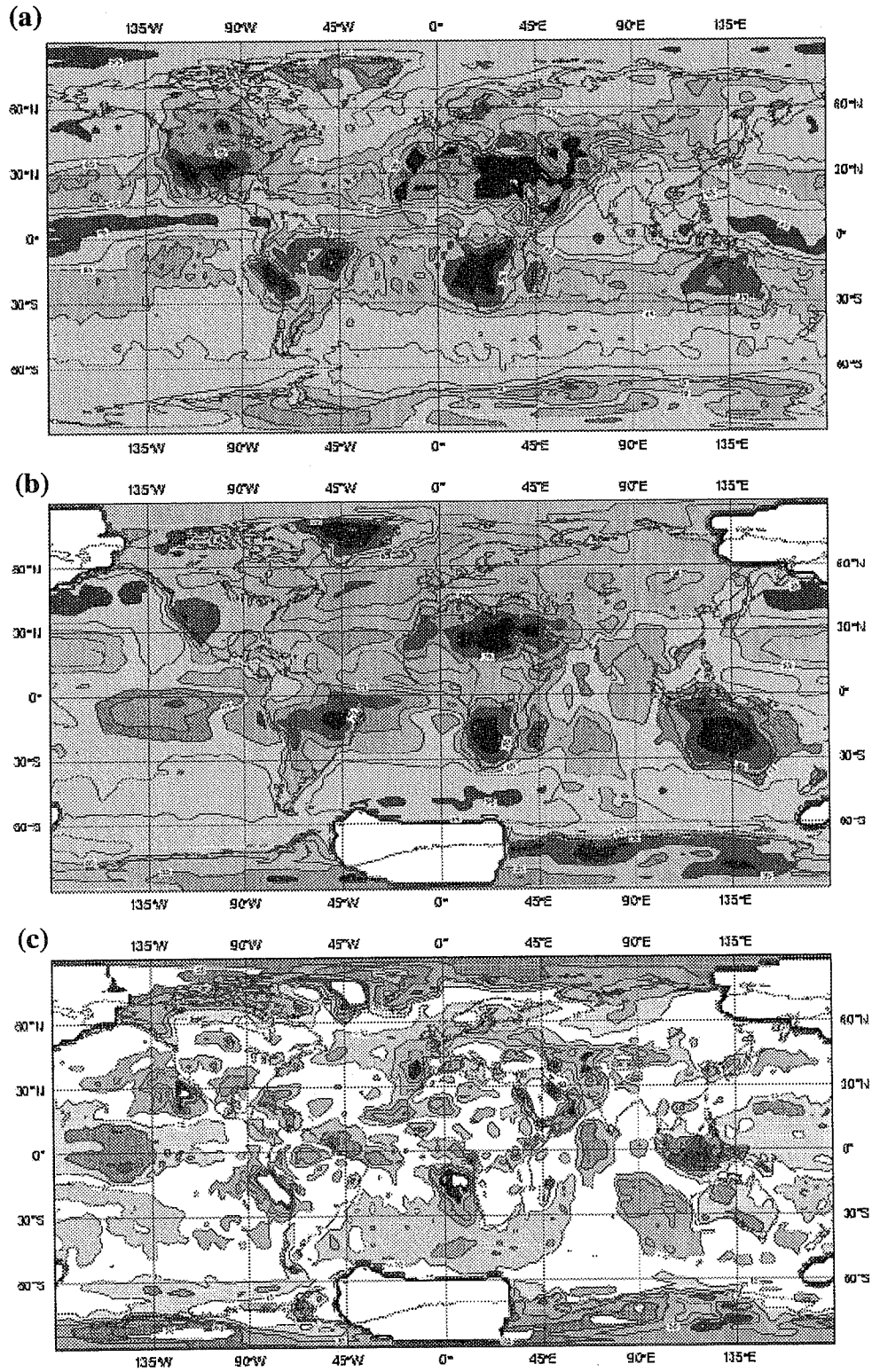

Fig. 7.1-9 (a) shows the total cloud cover [%] using the CONTROL scheme. (b) shows the estimated cloud cover given by the International Satellite Cloud Climatology Project (ISCCP). (c) shows the differences of the two global datasets. The data covers the three month period (June/July/August, 1987).

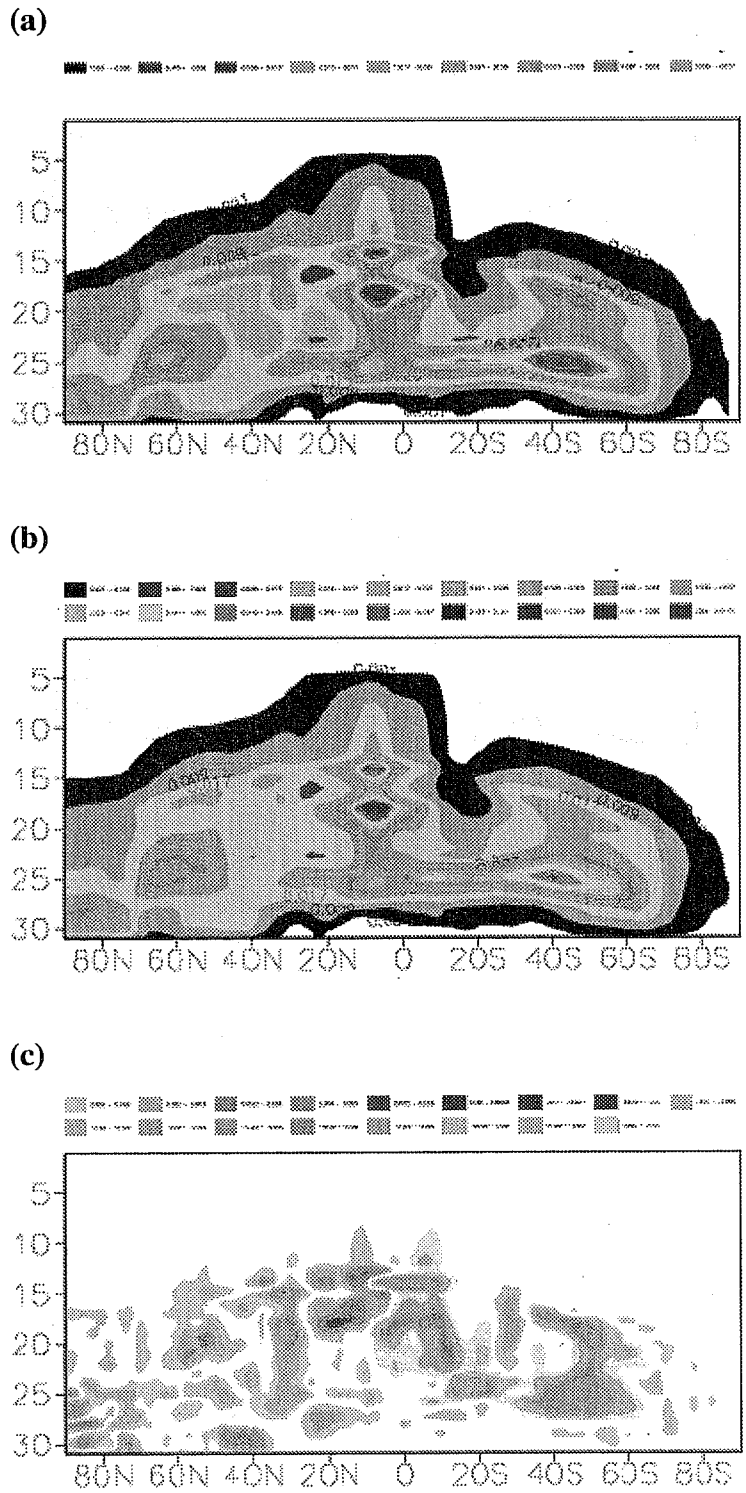

Fig. 7.1-10 Zonal mean cross-section of cloud liquid water and ice [kg/kg] comparing (a) the CONTROL scheme with (b) the SLAVEPP scheme. (c) shows the differences between (a) and (b). The data covers the three month period (June/July/August, 1987).

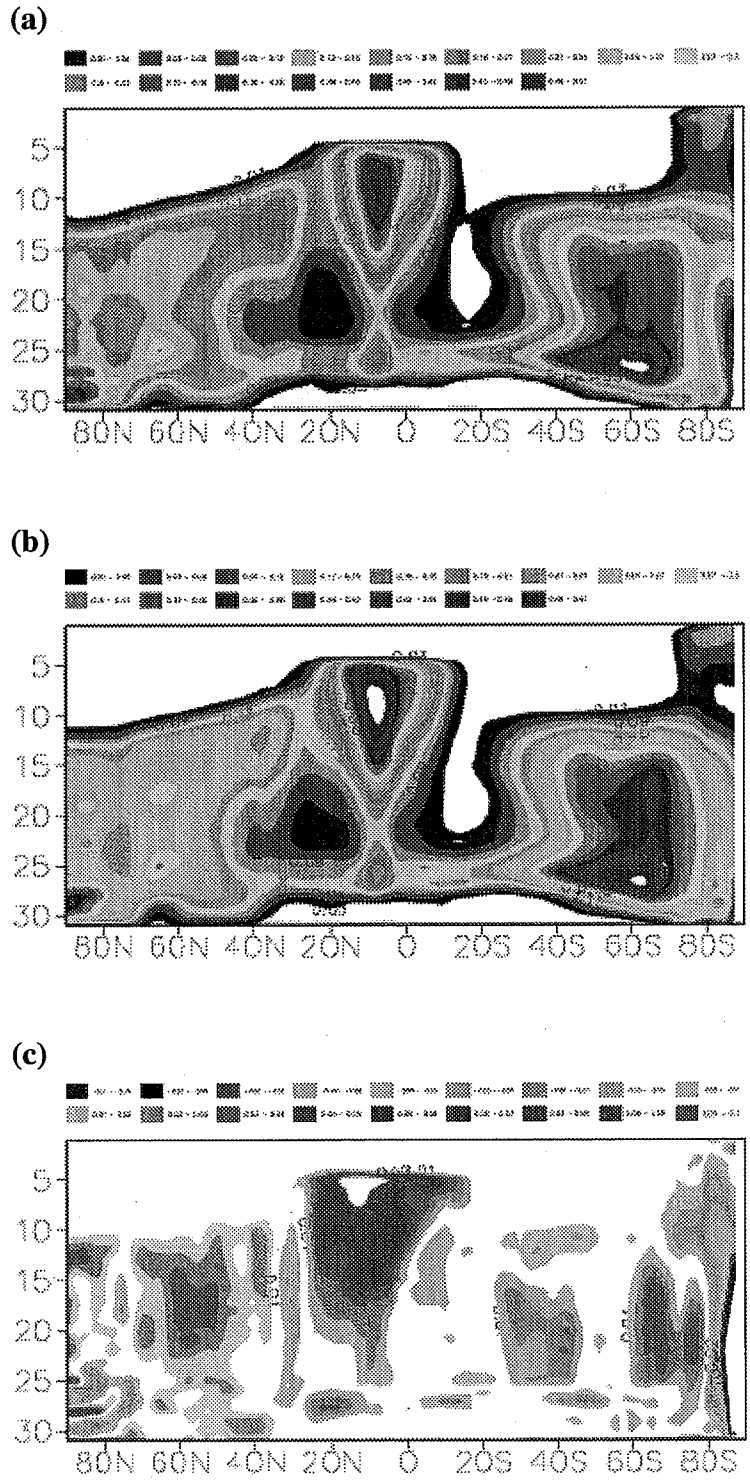

Fig. 7.1-11 Zonal mean cross-section of cloud fraction [%] comparing (a) the CONTROL scheme with (b) the SLAVEPP scheme. (c) shows the differences between (a) and (b). The data covers the three month period (June/July/August, 1987).

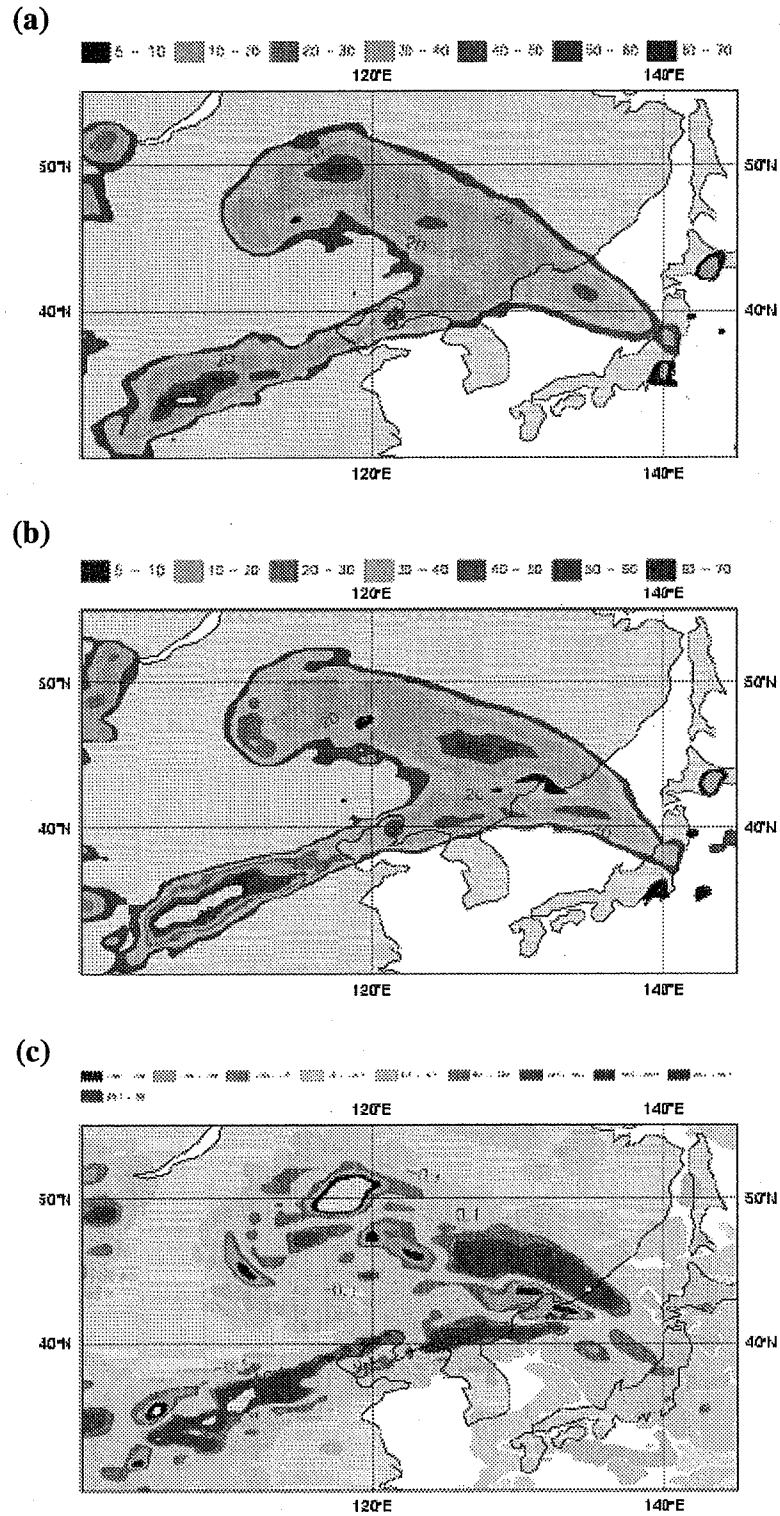

Fig. 7.1-12 24h accumulated total rainfall [mm/day] (a) after 72 hours of forecast using the SLAVEPP scheme compared to (b) the operational forecast from the 4.07.1998 12Z (48h-72h) in East Asia. (c) shows less forecasted precipitation when using the SLAVEPP scheme compared to the CONTROL method.

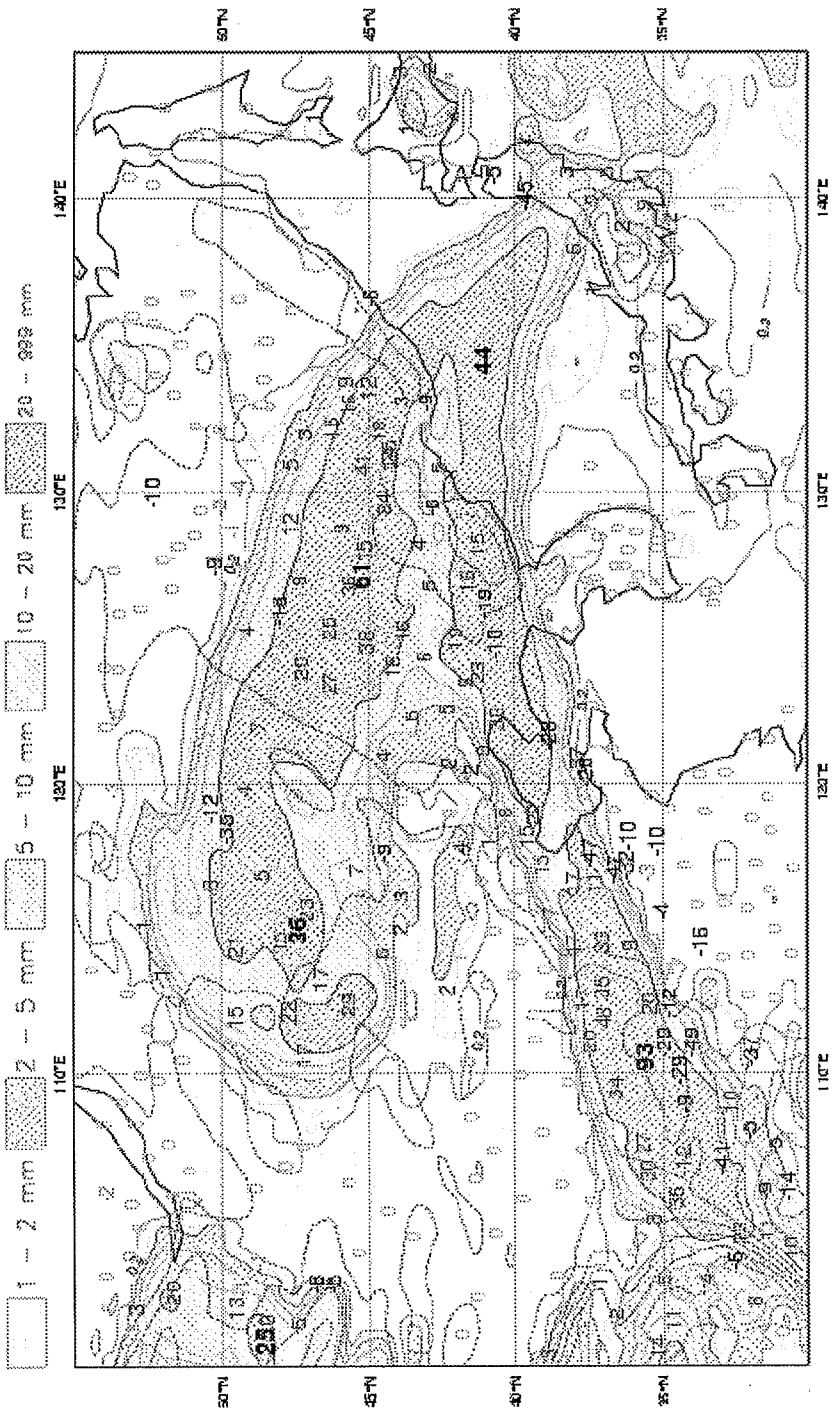

Fig. 7.1-13 Mean forecast error of the operational forecast using the CONTROL scheme. It shows the errors of the 24h accumulated total rainfall [mm/day] with respect to the observations from the 4.07.1998 12Z (48h-72h) in East Asia. The small numbers represent forecast biases. Big numbers represent forecasted total rainfall amount in mm/day.

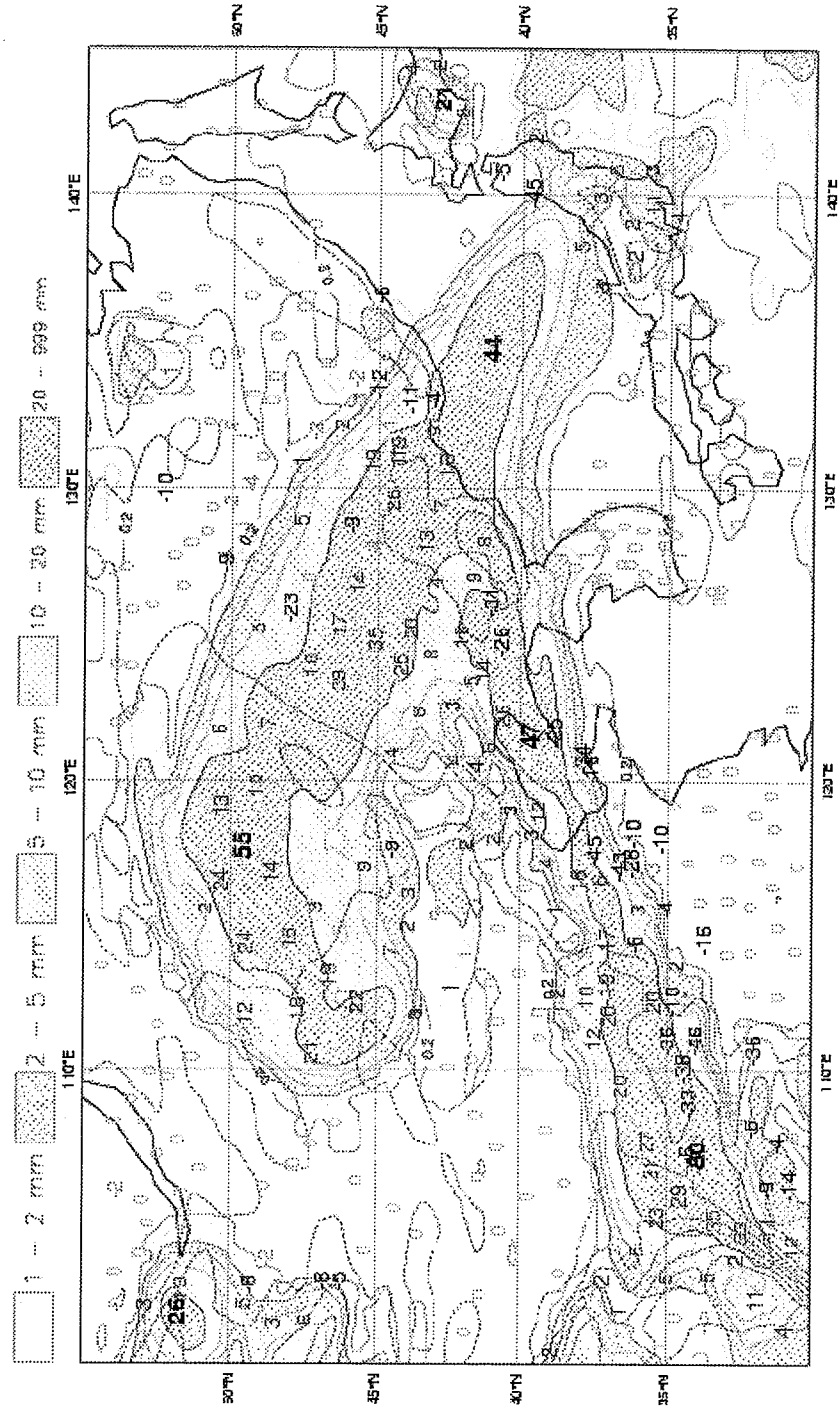

Fig. 7.1-14 Mean forecast error of the forecast using the SLAVEPP scheme. It shows the errors of the 24h accumulated total rainfall [mm/day] with respect to the observations from the 4.07.1998 12Z (48h-72h) in East Asia. The small numbers represent forecast biases. Big numbers represent forecasted total rainfall amount in mm/day.